Success of GDNF-based treatment of Hirschsprung disease depends on NCAM1 signaling and various subtypes of enteric neural progenitors

Alassane Gary [1,2,#], Rodolphe Soret [1,2,#,*], Marie A. Lefèvre [1,2], Nejia Lassoued [1,2], Ann Aspirot [3,4], Christophe Faure [2,3,5], Nicolas Pilon [1,2,3,*]

[1] Département des Sciences Biologiques, Université du Québec à Montréal, Montréal, Québec, Canada

[2] Centre d'excellence en recherche sur les maladies orphelines – Fondation Courtois (CERMO-FC), Université du Québec à Montréal, Montréal, Québec, Canada

[3] Département de pédiatrie, Université de Montréal, Montréal, Québec, Canada

[4] Division de chirurgie pédiatrique, Centre hospitalier universitaire Sainte-Justine, Montréal, Québec, Canada; Département de pédiatrie, Université de Montréal, Montréal, Québec, Canada.

[5] Division de gastroentérologie, hépatologie et nutrition pédiatrique, Centre Hospitalier Universitaire Sainte-Justine, Montréal, Québec, Canada; Département de pédiatrie, Université de Montréal, Montréal, Québec, Canada.

[#] *equal contribution*

**e-mail: soret.rodolphe@uqam.ca; pilon.nicolas@uqam.ca*

ABSTRACT

Hirschsprung disease (HSCR) is a deadly congenital disorder where the enteric nervous system (ENS) is absent from the distal bowel. Current surgical treatment is generally life-saving but is often accompanied by long-term bowel problems and comorbidities. As alternative, we are developing a regenerative therapy based on rectal administration of the neurotrophic factor GDNF. We previously showed that administering GDNF enemas to HSCR mice soon after birth suffice to permanently induce a new ENS from tissue-resident neural progenitors. Here, we clarify the underlying mechanism using single-cell transcriptomics, signal transduction inhibitors and cell lineage tracing tools. Notably, we found that the neurogenic effect of GDNF is mediated by NCAM1, rather than by its canonical signaling receptor RET. We also unveiled the existence of multiple differentiation pathways that involve a larger than expected repertoire of tissue-resident neural progenitors, including a surprising one not derived from the usual neural crest.

INTRODUCTION

The enteric nervous system (ENS) is a wide network of interconnected neural ganglia that spans the entire gastrointestinal tract, controlling motility and many other gastrointestinal functions [1-3]. Both neurons and glia of the ENS are derived from neural crest cell (NCC)-derived progenitors that colonize the bowel during pre-natal development [4,5]. Most ENS progenitors originate directly from vagal NCCs, which enter the foregut mesenchyme and then migrate toward the hindgut to eventually colonize the entire gastrointestinal tract [6,7]. When this developmental process fails, ENS ganglia are lacking in the rectum and over varying lengths of the colon, a severe birth defect known as Hirschsprung disease (HSCR) [5,8,9]. NCC-derived Schwann cell precursors (SCPs) constitute another important source of ENS progenitors, which in this case use extrinsic nerves as entry points to colonize the developing bowel, mainly in the colon, and after birth [10,11]. However, although extrinsic innervation of the aganglionic colon is more abundant than normal in the context of HSCR [12], the accompanying increase in SCPs cannot spontaneously compensate for the lack of the vagal NCC-derived pool [13].

Current treatment of HSCR involves surgical removal of the bowel segment lacking ENS ganglia (aganglionic), a procedure that is generally life-saving for most affected children [14,15]. However, postoperative bowel problems are common and can significantly impact the patient's quality of life [14,16-18]. Using genetically distinct mouse models of HSCR, we are developing a non-surgical alternative to this imperfect treatment, based on post-natal stimulation of tissue-resident ENS progenitors[19,20]. We demonstrated that daily rectal administration of GDNF (glial cell line-derived neurotrophic factor) for only 5 days, from post-natal day (P)4 to P8, can regenerate the missing ENS in the colon, with long-term benefits on overall colon function and mouse survival [19]. Moreover, GDNF promoted *de novo* neurogenesis in human colonic explants obtained from HSCR surgery and cultured *in vitro* [19]. Our mechanistic studies suggested that the ENS-inducing effect of GDNF is at least in part due to its ability to mobilize SCPs from extrinsic nerves and cause them to differentiate into enteric neurons and glia [19]. Yet, our findings also raised many important mechanistic questions that could not be addressed in this prior study. Notably, the identity of the signaling pathway(s) mediating the neurogenic effect of GDNF in this context as well as the presumed presence of non-SCP sources of ENS progenitors had not been experimentally investigated.

During normal pre-natal ENS development, GDNF greatly influences the migration, proliferation and neuronal differentiation of vagal NCCs via the transmembrane tyrosine kinase RET (Rearranged during transfection), upon binding to the co-receptor GFRα1 (GDNF family receptor, alpha 1) [21-24]. This is reflected in the genetics of HSCR, where *RET* variants are the main genetic risk factor of this multifactorial disease [25,26], raising reasonable doubts about global applicability of GDNF-based therapy. That being said, in the most frequent short-segment form of HSCR, associated *RET* variants are typically non-coding, affecting RET protein levels, not function [27,28]. Therefore, as exogenous

GDNF can activate an autoregulatory loop of endogenous GDNF/RET expression in the aganglionic colon [19], these cases should nonetheless be treatable with GDNF enemas. Moreover, in the Schwann cell lineage, GDNF-bound GFRα1 instead signals through NCAM1 (Neural cell adhesion molecule 1) [29,30], suggesting that RET could in fact even be dispensable for mediating the postnatal ENS-inducing effects of GDNF in the context of HSCR. Clearly, addressing this question will be key for advancing GDNF-based therapy closer to clinical application. A better understanding of the cellular heterogeneity among tissue-resident ENS progenitors is also warranted. Current data suggest that about two-thirds of GDNF-induced neurons are not derived from SCPs. Identifying these non-SCP ENS progenitors would allow to better evaluate the requirement for RET signaling, and perhaps also explain how the GDNF-induced ENS is properly balanced in terms of neuron subtypes [19] despite the fact that the progeny of SCPs is normally biased toward a cholinergic phenotype [10].

Using single-cell transcriptomics, small molecule-based perturbation of signaling pathways, and a wide range of genetic cell lineage tracing tools, we here provide evidence that RET is dispensable for mediating the neurogenic effect of GDNF in the distal colon of HSCR mice, and that this region contains at least three subtypes of tissue-resident ENS progenitors with complementary differentiation potential, including one unexpected subtype that is not derived from the NCC lineage.

RESULTS

GDNF treatment changes the relative proportion of neural cell subpopulations in the distal colon of *Hol*$^{Tg/Tg}$ mice

To better understand the mechanism of GDNF-induced neurogenesis in the otherwise aganglionic colon of HSCR mice, we turned to single-cell RNA sequencing (scRNA-seq). For these mechanistic studies, we continued to focus on the *Holstein* mouse model for trisomy 21 (collagen VI upregulation)-associated HSCR [31-33]. This model significantly outperforms two other models available in our laboratory in terms of either phenotypic penetrance of megacolon (compared to incomplete male-biased penetrance in the *TashT* line [34]) or fertility rate (compared to subfertility in the *Piebald-Lethal* line [35]) – both of which being also responsive to GDNF treatment [19]. To facilitate recovery of ENS cells, we bred *Holstein* mice with the *G4-RFP* transgenic line [36]. The *G4-RFP* reporter is known to label most neural crest derivatives with the red fluorescent protein (RFP) DsRed2 during pre-natal development, including ENS progenitors [32,36,37]. To validate that this transgene is still active after birth, we immunolabeled the distal colon of P10 *Hol*$^{Tg/Tg}$*;G4-RFP* double transgenic mice that were previously treated with GDNF enemas between P4-P8, looking for the presence of RFP-labeled HuC/D+ neurons and SOX10+ glia. This analysis revealed that RFP marks 88% of SOX10+ enteric glia-like cells (including extrinsic nerves-associated SCPs) and 70% of HuC/D+ enteric neurons at this stage (Fig.S1a). We then proceeded with the scRNA-seq analysis using the same experimental setup, but now also including untreated *Hol*$^{Tg/Tg}$*;G4-RFP* (Fig.S1b). We recovered RFP+ cells from the distal colon (including the aganglionic segment and part of the transition zone) of 6 untreated and 8 GDNF-treated mouse pups by fluorescence-activated cell sorting (FACS), after which individual cells were processed using the 10x Genomics platform (Fig.1a). This approach yielded 3684 and 6352 high-quality cells from untreated and GDNF-treated *Hol*$^{Tg/Tg}$*;G4-RFP* mice, respectively (Fig.S2a-b). Using the Trailmaker software, these cells were regrouped in 19 cell clusters, which are present in both untreated and GDNF-treated datasets (Fig.S2a-d). Seven of these clusters were associated with the ENS, with three being assigned an SCP identity (expressing specific markers like *Dhh, Mpz, Mbp* and *Egfl8*), two being assigned an enteric glial cell (EGC) identity (expressing specific markers like *Nell2, Col20a1, Ccn2* and *Cpe*), and another two being assigned an enteric neuron identity (expressing general markers *Elavl4, Tubb3,* and *Gap43*). Remaining cell clusters were generally smaller and not directly associated with the ENS, including specific groups of lymphoid, myeloid, vascular, epithelial and smooth muscle cells, as well as a more general group of proliferating cells (expressing *Pcna* and/or *Mki67*) (Fig.S2a-d). To refine our analysis, we only selected cells that express either the pan-neuronal marker *Elavl4* or the pan-glial and ENS progenitor marker *Sox10*, leaving 1354 and 3006 high-quality cells from untreated and GDNF-treated *Hol*$^{Tg/Tg}$*;G4-RFP* mice, respectively. Unsupervised reclassification of these ENS-associated cells revealed 14 distinct clusters representing

subpopulations of SCPs (three clusters, including one with mixed EGC identity), EGCs (eight clusters, including three proliferating) and enteric neurons (three clusters) (Fig.1b-c), which are again present in both untreated and GDNF-treated groups (Fig.1e). Analysis of the relative proportion of the different clusters revealed a marked enrichment in enteric neurons and proliferating *Mki67*$^{+}$ EGCs in the GDNF-treated group, which occurred mainly at the expense of SCPs and cells with mixed SCP/EGC identity (Fig.1f). These observations are highly consistent with our prior discovery that the GDNF-induced ENS is at least in part derived from SCPs [19], thereby making this dataset a reliable resource to better understand the underlying mechanism.

The neurogenic effect of GDNF is mediated by the NCAM1/FAK signaling pathway

We first took advantage of our scRNA-seq data to examine the expression profile of GDNF receptor-coding genes, focusing on the GDNF-treated *Hol*$^{Tg/Tg}$*;G4-RFP* dataset. This analysis revealed a striking difference for the signaling receptors, with *Ncam1* highly expressed in all cell clusters, while *Ret* expression appears limited to a subset of enteric neurons only (Fig.2a). The binding receptor-coding genes *Gfra1* and *Gfra2* were also found to be widely expressed, with a partly overlapping and complementary distribution (Fig.2a). *Gfra3* expression appeared restricted to SCP clusters, whereas weak *Gfra4* expression could only be detected in a few neurons (Fig.2a). As GDNF can bind either GFRa1 or GFRa2 [38], these observations strongly suggest that GDNF binds either one and then signals through NCAM1 to make new neurons from SCPs and perhaps other ENS progenitors within the EGC clusters. To further validate this possibility, we evaluated the distribution of the NCAM1 protein and its downstream signaling effector phospho-FAK[Y397] in the distal colon of *Hol*$^{Tg/Tg}$ mice over time, before ($P4_{[0h]}$), during ($P4_{[6h]}$ and P6) and after (P10) the end of GDNF treatment. NCAM1 is already present in SOX10+ cells before the start of GDNF treatment at P4, both within and outside extrinsic nerve fibers (Fig.2b). As soon as 6h after the start of GDNF treatment, NCAM1 proteins levels then increase over time, with high levels being maintained even two days after completion of the GDNF treatment period, which ends at P8. Phospho-FAK[Y397] levels are lower in these SOX10+ cells before the start of GDNF treatment, but then similarly increase over time (Fig.2b). Hence, these additional observations also suggest GDNF-induced autoregulation of NCAM1, as we previously showed for RET [19].

To confirm the relative importance of NCAM1 *vs.* RET in mediating the neurogenic effect of GDNF in the colon of *Hol*$^{Tg/Tg}$ mice, we next verified the efficacy of GDNF treatment in presence of chemical inhibitors that prevent the phosphorylation of FAK (PF-562271)[39] and RET (BLU-667)[40], respectively. Each of these inhibitors was administered via daily i.p. injections (30 mg/kg) during the GDNF enema treatment period (P4-P8), and impact on colon tissues was then assessed 6h after the last enema/injection at P8. Western blot analysis of full-thickness proximal/mid colon confirmed efficacy of

each inhibitor (Fig.S3), while further highlighting that RET is poorly activated in this context compared to a control tissue with robust endogenous GDNF-RET activity like the adult hypothalamus [41] (Fig.S3c). Accordingly, immunofluorescence staining of the distal colon segment from the same samples revealed that phospho-RET[Y1062] inhibition with BLU-667 has no impact on GDNF-induced neurogenesis. In marked contrast, phospho-FAK[Y397] inhibition with PF-562271 led to a significant decrease in the number of GDNF-induced neurons per mm² (Fig.2c). These data confirm that the NCAM/FAK signaling pathway is crucial for GDNF-induced neurogenesis in the aganglionic colon of HSCR mice.

GDNF-induced neurogenesis from SCPs partly involves an intermediary EGC-like state

We reasoned that our scRNA-seq data would also be helpful to identify additional sources of GDNF-induced neurons, other than SCPs [19]. Indeed, as some EGCs behave as ENS progenitors with a neurogenic potential under certain conditions [42-46], we hypothesized that at least one of the many subgroups of EGCs in our analysis of P10 mice would contain such progenitors. To reveal the presence of these neuronal-fated progenitors in our scRNA-seq data, we verified the expression pattern of the pan-neuronal marker *Elavl4*, predicting that it should be upregulated while the EGC transcriptional program is still active. Again focusing on the GDNF-treated *Hol*$^{Tg/Tg}$*;G4-RFP* dataset, this analysis confirmed the presence of several *Elavl4* expressing cells among both the SCP and EGC clusters, in addition to all enteric neuron clusters (Fig.3a). Reclustering these *Elavl4* expressing cells then unveiled an intriguing connection between SCP, EGC and enteric neuron clusters (Fig.3b-d). This linear relationship was validated by a pseudotime trajectory analysis using the monocle algorithm[47], which further confirmed that it exists in the untreated *Hol*$^{Tg/Tg}$*;G4-RFP* dataset as well (Fig.3e) – most likely reflecting the presence of the ENS-containing transition zone in our samples. Moreover, we observed a similar linear connection when reclustering was based on *Tubb3* expression instead of *Elavl4* (Fig.S4), with overall inverse expression gradients of *Sox10* and these neuronal markers. All these analyses consistently point to a stepwise differentiation model (Figs.3c-d and S4c-d) whereby a subset of SCPs (expressing *Dhh*, *Mpz, Mbp* and *Egfl8*) progressively loose their Schwann cell lineage identity to differentiate into EGCs expressing *Nell2, Col20a1* and *Ajap1* (SCP/EGC and EGC #a clusters), then EGCs expressing *Ccn2*, *Col9a2* and *Igfbp4* (EGC #b cluster), and finally enteric neurons expressing general markers like *Phox2b, Tubb3* and *Gap43,* as well as different combinations of subtype-specific markers like *Chat, Nos1, Vip* and *Calcb* (EN #a-f clusters). Interestingly, we further noted that cells from the EGC #b cluster also expresses *Gfap*, *Slc18a2, Sox2* and *Cpe* (Figs.3c-d and S4c-d). These genes were recently reported to collectively characterize EGCs poised for neurogenesis in the small intestine of *Plp1-GFP* mice at P14 [48]. Moreover, these poised EGCs were

most recently assigned to the “EG 1-2” clusters identified in human ileum and colon biopsies from children without an intestinal motility disorder [49].

To validate the stepwise differentiation model described above at both genetic and protein levels, we then turned again to a cell lineage tracing system that previously allowed us to follow the progeny of *Dhh*-expressing SCPs in *Hol*$^{Tg/Tg}$ mice treated with GDNF [19]. In these GDNF-treated triple-transgenic *Hol*$^{Tg/Tg}$ pups also bearing the *Dhh-Cre* transgene [50] and the *R26R-YFP* reporter allele [51] (*Hol*$^{Tg/Tg}$*;Dhh-Cre*$^{Tg/+}$*;R26*$^{YFP/+}$), we now evaluated the presence of SCP-derived cells co-expressing either GFAP or SLC18A2 proteins together with the early enteric neuron marker PHOX2B in the distal colon at P10 (*i.e.* 2 days after the last GDNF enema, as for the scRNA-seq study). Triple-immunofluorescence staining clearly shows that GDNF-induced ENS ganglia contain several of these SCP-derived (YFP+) cells that are differentiating into PHOX2B+ enteric neurons while still expressing the EGC markers GFAP (Fig.4a) or SLC18A2 (Fig.4b). Yet, quantitative analysis as a function of time revealed that GFAP-positive cells are not all derived from *Dhh*-expressing SCPs on the first day of GDNF treatment at P4 (Fig.4c). Furthermore, this kinetic analysis highlighted a progressive decline of GFAP protein expression in SCP-derived cells during ($P4_{[6h]}$ and P6) and after (P10 and P20) GDNF treatment, with a mean of 87% of YFP+ cells per ganglion also positive for GFAP after the first 6 hours of treatment to a mean of 31% at P20 (Fig.4c). This progressive decline most likely reflects the inverse progression of neuronal differentiation, as the GFAP protein is no longer detectable in SCP-derived cells that stain positive for the late neuronal marker HuC/D in GDNF-induced ganglia at P20 (Fig.S5). Collectively, these results support the notion that some extrinsic nerve-associated SCPs can differentiate into enteric neurons by transitioning through an EGC-like state.

GDNF-induced neurogenesis is quicker from SCPs than from EGCs and persists beyond the treatment period

To clarify the relationship between colonic SCPs and EGCs in response to GDNF treatment of *Hol*$^{Tg/Tg}$ mice, we extended our cell lineage tracing studies by comparing the kinetic profile of GDNF-induced neurogenesis from *Dhh*-expressing SCPs as well as from EGCs expressing either *Gfap* (with the tamoxifen-inducible *GFAP-CreERT2* driver)[52] or *Slc18a2* (with the *Slc18a2-Cre* driver)[53]. Like most of our other kinetic analyses, we analyzed one time point just before treatment begins ($P4_{[0h]}$), two time points during the GDNF treatment period ($P4_{[6h]}$) and P6), and two time points after the end of treatment (P10 and P20) (Fig.5a). This analysis first revealed that, regardless of their origin, HuC/D+ neurons in the distal colon become detectable by immunofluorescence remarkably quickly, as early as 6h after the start of treatment (Fig.5b). Otherwise undetectable in this region without exposure to GDNF, these HuC/D+ neurons begin to appear either isolated or organized into very small ganglia (Figs.5c-d). At this very early stage, they are detected in all colon samples of GDNF-treated pups, but

not in all fields of view of the microscope when using a 60x objective. After this $P4_{[6h]}$ time point, the mean density of HuC/D+ neurons per mm^2 increases in a steady manner and, surprisingly, even well after the end of the 5-day GDNF treatment period (P4-P8), until at least P20 (Fig.5b).

When considering the Cre driver used for cell lineage tracing, our comparative kinetic analysis revealed that *Dhh*-expressing SCPs are among the first newly generated HuC/D+ neurons, after only 6h of GDNF treatment (Fig.5c). GDNF-induced neurogenesis appeared to be considerably delayed in EGCs expressing either *Slc18a2* (Fig.5d) or *Gfap* (Fig.5e), with first detection of HuC/D+ neurons at P6 and P10, respectively. On the one hand, this delay supports the stepwise differentiation model (SCP → EGC → enteric neurons) described above (Figs.3-4). On the other hand, as *Gfap*-expressing EGCs most likely exist independently of the SCP lineage (Fig.4c), it also suggests that neuronal differentiation is slower from EGCs than from SCPs. After first detection, the percentage of YFP+ neurons then increases over time with all three Cre drivers, in a way roughly similar to the overall time-dependent increase in neuronal density (Fig.5b), with final contribution at P20 reaching between 27-39% of all GDNF-induced neurons (Fig.5c-e). Hence, most neurons originating from SCPs and/or EGCs (at least those labeled with our cell lineage tracing tools) seem to be generated after the end of the GDNF treatment period. In other words, most of the neurons that first appear in response to GDNF likely have another origin, distinct from SCPs or EGCs.

Direct transdifferentiation is the preferred mode of neurogenesis in response to GDNF, regardless of the targeted subtype of ENS progenitors

The rapid neuronal differentiation uncovered at $P4_{[6h]}$ (Fig.5b) strongly suggested that the first GDNF-induced neurons that appear in the distal colon of $Hol^{Tg/Tg}$ mice are the result of direct transdifferentiation, without cell division. To validate this hypothesis and more globally evaluate the contribution of such direct neuronal conversion, we conducted EdU incorporation assays in GDNF-treated $Hol^{Tg/Tg}$ pups, again as a function of time and subtypes of ENS progenitors (SCPs *vs.* EGCs). Daily EdU treatment began at P3 and continued throughout the duration of the GDNF treatment period (P4-P8) (Fig.6a). As expected, immunofluorescence staining of distal colon samples showed that EdU incorporation into GDNF-induced HuC/D+ neurons was extremely rare at $P4_{[6h]}$ (Fig.6b), in contrast to the numerous proliferative cells in their vicinity. We found only two neurons in total, from the same mouse, that stained positive for EdU at this stage (Fig.S6). Extending this global analysis at later time points revealed a time-dependent increase in EdU+ neurons, but these always remained the minority, resulting in consistently high percentages (>67%) of direct conversion, both during (P6) and after (P10 and P20) the period of GDNF treatment (Fig.6b). Similar trends can be observed when data are analyzed based on the Cre driver used for lineage tracing of SCPs and EGCs (Fig.6c-e). Percentages of EdU-negative neurons are always the highest at first detection of YFP+ neurons, with relative levels

being inversely proportional to the stage at which this occurs in each mouse line: 100% at $P4_{[6h]}$ for *Dhh*-expressing SCPs (Fig.6c), 91% at P6 for *Sclc18a2*-expressing EGCs (Fig.6d), and 77% at P10 for *Gfap*-expressing EGCs (Fig.6e). These data offer a plausible mechanism to explain the rapid generation of GDNF-induced neurons after just 6h of treatment, while also indicating that direct transdifferentiation remains the preferred mode of neurogenesis irrespective of temporal constraints.

A neural crest-independent subtype of ENS progenitors appears necessary to balance overall cholinergic and nitrergic differentiation of GDNF-induced neurons

In a final set of experiments, we sought to determine the specific contribution of SCPs and EGCs to the WT-like diversity of neuronal subtypes that we know GDNF can generate in the distal colon of $Hol^{Tg/Tg}$ mice [19]. Using the same cell lineage tracing tools as described above, we here focused on the co-expression of YFP and HuC/D with either ChAT (choline acetyltransferase) or NOS1 (nitric oxide synthase 1) as markers of the main subtypes of excitatory and inhibitory motor neurons, respectively. Strikingly, our analyses at P20 showed that the vast majority of YFP+ neurons derived from either *Dhh*-expressing SCPs or *Gfap*-expressing EGCs are also positive for ChAT, with proportions of 83% and 80%, respectively (Figs.7a). Much smaller percentages of YFP+ neurons were found to co-express NOS1, with averages of 12% for those derived from *Dhh*-expressing SCPs and 14% from *Gfap*-expressing EGCs (Fig.7a). Similar trends were noted with the *Slc18a2*-Cre driver (Fig.S7), with a slightly higher percentage of nitrergic neurons that most likely reflects, at least in part, *Slc18a2* expression in a subset of these neurons (Fig.1d). When compared to each other, data for *Dhh*-expressing SCPs and *Gfap*-expressing EGCs result in cholinergic to nitrergic ratios of 6.3 : 1 on average, which is much greater than the WT-like ratio of 1.2 : 1 previously reported for all GDNF-induced HuC/D+ neurons (52% ChAT+ *vs*. 42% NOS1+) [19]. This ratio difference led us to think that the additional subtype of ENS progenitors already predicted from our temporal cell lineage tracing data (Fig.5) must be more prone to differentiate into nitrergic neurons.

To verify the possibility that this presumed additional subtype of ENS progenitors could be derived from NCCs but was simply missed by our cRNA-seq strategy based on the *G4-RFP* transgene (Fig.1a), we traced all NCC derivatives in the colon using the *Wnt1-Cre2* driver [54]. When used in conjunction with the *R26R-YFP* reporter allele [51] ($Wnt1\text{-}Cre2^{Tg/+};R26^{YFP/+}$), this “pan-NCC” Cre driver normally enables YFP expression in virtually all enteric neurons and EGCs of the distal colon at P20, as we confirmed ourselves (Fig.7b). However, this was not the case when the same system was used in the *Holstein* mutant background. To our astonishment, after GDNF treatment between P4-P8, about a quarter of newly induced HuC/D+ neurons were found to be negative for YFP in the distal colon of these $Hol^{Tg/Tg};Dhh\text{-}Cre^{Tg/+};R26^{YFP/+}$ mice at P20 (Fig.7b). This ENS contribution from a non-NCC source seems to be strongly oriented toward neurons, as less than 3% of SOX10+ EGCs were

similarly negative for YFP in the same GDNF-treated animals (Fig.7b). As expected from the phenotypic analysis of neurons derived from *Dhh*-expressing SCPs and *Gfap*-expressing EGCs (Fig.7a), this atypical non-NCC-related subtype of ENS progenitors appeared ~4X more prone to differentiate into nitrergic neurons, now yielding roughly equal proportions of NOS1+ and ChAT+ neurons (Fig.7c). These data indicate that there are at least three subtypes of ENS progenitors (four, if we consider *Gfap*-expressing and *Slc8a2*-expressing EGCs separately) with complementary differentiation potential in the aganglionic colon. Although not all ENS progenitors appear to originate from NCCs, all can be stimulated by GDNF.

DISCUSSION

A few years ago, we reported the amazing discovery that GDNF can promote *de novo* neurogenesis in the otherwise aganglionic colon of HSCR mice as well as in surgical explants of human patients [19]. With the current study, we greatly deepen our understanding of the underlying mechanism, which turns out to be more complex than initially thought. As summarized in Fig.8 and discussed in more detail below, there are a lot of fascinating findings to keep in mind. Just a few hours after rectal administration, GDNF triggers a robust neurogenic response in the colon, which then persists for several days even when GDNF is no longer administered. This GDNF-induced neurogenic program appears to be mediated by NCAM1-FAK signaling, not by RET. Within the aganglionic colon, at least three distinct subtypes of ENS progenitors are likely involved, and all need to be stimulated in a coordinated way to ensure enteric neuronal diversity in well-balanced proportions. Most surprisingly, one of the identified subtypes of ENS progenitors seems not to derive from NCCs as all ENS-related cells normally do.

RET is dispensable for GDNF-induced neurogenesis in the aganglionic colon

GDNF-RET signaling is critical for normal ENS formation from vagal NCCs [55,56], explaining why *RET* variants are among the main genetic risk factors for HSCR [27,57,58]. However, modeling this association in mice has proved difficult. Indeed, the impact of *Ret* deficiency on the murine ENS is either benign at the heterozygous state [59] or too severe at the homozygous state (total intestinal aganglionosis) [56]. Distal colon aganglionosis mimicking short-segment HSCR can be induced by treating hypomorphic *Ret*$^{9/-}$ mice with mycophenolate mofetil [60], but the general toxicity associated with this compound prevented us from evaluating GDNF effect in this context [19]. Here, we used a pharmacological approach to circumvent these problems, demonstrating that RET activity is dispensable for mediating the neurogenic effect of GDNF in the aganglionic colon of the *Holstein* mouse model. This result is also consistent with our scRNA-seq data showing that *Ret* expression is mostly restricted to a subset of induced neurons only. In marked contrast, the same transcriptome data revealed that *Ncam1* is robustly expressed in virtually all ENS progenitors and induced neurons, and pharmacological inhibition of the NCAM1-FAK signaling axis significantly impaired the neurogenic effect of GDNF.

NCAM1 was already known to influence ENS gangliogenesis before birth [61], and to mediate GDNF effects in the Schwann cell lineage after birth [29]. Our new mouse data now suggest that NCAM1 also mediates GDNF effects in postnatal EGCs as well, at least in the context of aganglionosis. There is also cumulative circumstantial evidence that NCAM1 can similarly mediate GDNF signaling in human tissues. In particular, NCAM1 (also known as CD-56) has been recently reported as a reliable marker for FACS-mediated recovery of ENS cells from human postnatal gastrointestinal tissues [62], including aganglionic samples obtained from children with HSCR [49]. ScRNA-seq data generated from these

NCAM1+ cells (also positive for the additional marker CD-90) revealed the presence of both SCPs (referred to as Schwann-like enteric glia) and EGCs (referred to as canonical enteric glia) in aganglionic samples [49]. These transcriptomic data are also supported by our own immunofluorescence analyses of human aganglionic samples, which show robust NCAM1 protein expression both within (presumably in SCPs) and outside (presumably in EGCs) βIII-Tubulin+ extrinsic nerves (Fig.S8).

The reason why RET is present in a subset of GDNF-induced neurons is unclear. RET is normally present in a subset of adult enteric neurons as well, but a recent study based on two distinct conditional mutant mouse lines (*Vip*$^{Cre/+}$;*Ret*$^{Flox/Flox}$ and tamoxifen-inducible *Ret*$^{CreER/Flox\text{-}GFP}$) revealed that it is neither critical for cell survival nor for the control of gastrointestinal motility [63]. Combined with our previous and current data, these observations are reassuring about the global applicability of GDNF-based therapy. Even if RET was necessary for mediating the presumed beneficial effects of GDNF in non-ENS cells (*e.g.*, in epithelial cells [63,64]), it is noteworthy that HSCR-associated *RET* gene variants are generally predicted to reduce, but not abrogate, RET protein levels/activity [27,58]. In such cases with reduced RET levels/activity, GDNF-based therapy would nonetheless be highly valuable since GDNF enemas can trigger a feedback loop that increases protein levels of both RET and endogenous GDNF in the colon wall [19].

This increase in endogenous GDNF is also interesting in relation to the persistence of neurogenesis after the end of GDNF treatment. Whether this is the only reason, or whether it implicates another signalling pathway (or a combination of the two) is certainly worthy of investigation in future research.

The aganglionic colon is rich in ENS progenitors that can be directly converted into neurons by GDNF

The current study provides additional evidence that aganglionosis does not mean absence of ENS progenitors [65,66]. Both mouse (this study) and human [49] scRNA-seq data are consistent with the existence of two main progenitor subtypes that have the transcriptional signature of neural crest-derived SCPs or EGCs, as we further validated using several genetic cell lineage tracing tools. Yet, determining the exact contribution of each of these progenitor subtypes to the pool of GDNF-induced neurons is almost impossible to determine with currently available tools. For instance, we previously reported that ~10% of SCPs from the aganglionic colon are not fluorescently labeled when *R26R-YFP* reporter allele expression depends on the *Dhh-Cre* driver [19]. The tamoxifen-inducible nature of the *GFAP-CreERT2* also likely underestimates the neuronal contribution of EGCs beyond the tamoxifen administration window, whereas this contribution is likely overestimated with the *Slc18a2-Cre* driver that also has intrinsic neuronal activity. Above all, the portrait is greatly complicated by the SCP-EGC

lineage connection that we have uncovered. Based on the less specific *Wnt1-Cre2* driver, we can only conclude that ~75% of GDNF-induced neurons are collectively derived from NCCs.

Considering what we know about normal ENS development, this observation that not all GDNF-induced neurons are fluorescently labeled when using the pan-NCC *Wnt1-Cre2* driver was very surprising. The existence of a third subtype of ENS progenitors unrelated to NCCs is extremely intriguing, as is the observation that it differentiates preferentially into neurons rather than glial cells. The identity of this non-NCC-derived subtype of ENS progenitors that generate ~25% of GDNF-induced neurons is currently unknown and will certainly be the subject of exciting research in the near future.

Another intriguing discovery that was made during these studies is that direct transdifferentiation is the main mode of GDNF-induced neurogenesis regardless of ENS progenitor subtypes and time point relative to the treatment period. Yet, we also observed an increase of “indirect” differentiation via a dividing precursor over time, thereby most likely preventing GDNF to rapidly exhaust the pool of ENS progenitors. Such delayed response suggests that the pool of ENS progenitors is somehow protected by a quorum sensing-like mechanism that controls cellular density at tissue level, as observed in the immune system [67]. Regardless of the exact mechanism, the resulting two-step response is highly desirable from a therapeutic standpoint, as it allows to combine both rapid and long-lasting effects of the GDNF treatment. This knowledge will greatly help the design of clinical trials that we hope to undertake soon.

MATERIALS AND METHODS

Mice. *Holstein* (*Tg[Sox3-GFP,Tyr]HolNpln*) and *G4-RFP* (*Gata4p[5kb]-RFP*) transgenic lines were as previously described in our prior work [32,36]. *Dhh-Cre* (*FVB[Cg]-Tg[Dhh-cre]1Mejr/J*; JAX strain #012929), *GFAP-CreERT2* (*B6.Cg-Tg[GFAP-cre/ERT2]505Fmv/J*; JAX strain #012849) and *Wnt1-Cre2* (*B6.Cg-E2f1*$^{Tg(Wnt1\text{-}cre)2Sor}$*/J*; JAX strain #022501) mouse lines were purchased from the Jackson Laboratory (Bar Harbor, MM, USA), whereas the *Slc18a2-Cre* (*Tg[Slc18a2-Cre]OZ14Gsat/Mmucd*; MMRRC strain #034814-UCD) line was purchased from the Mutant Mouse Resource and Research Centers (MMRRC) at University of California, Davis. The Cre reporter line *Rosa26*$^{FloxSTOP\text{-}YFP}$ (*B6.129X1-Gt[ROSA]26Sor*$^{tm1(EYFP)Cos}$*/J*) was directly provided by Dr. Frank Costantini from Columbia University. All mice used in this study were maintained on the FVB/N genetic background, after at least 5 generations of backcrossing if acquired on a different background. All mice were housed and bred in individually ventilated cages within the conventional animal facility at the Université du Québec à Montréal, under a 12-hour light/dark cycle (7 AM to 7 PM) and with *ad libitum* access to Charles River Rodent Diet #5075 (Cargill Animal Nutrition). Genotyping was either made by visual inspection of coat color (for *Holstein* and *G4-RFP*) or standard PCR (for all Cre driver and reporter lines) using primers listed in Table S1. Euthanasia was performed using either CO_2 inhalation or decapitation (for pups aged of 10 days or less), both following isoflurane anesthesia. All experiments were approved by the Université du Québec à Montréal ethics committee (CIPA #959) and conducted in accordance with the Canadian Council on Animal Care (CCAC) guidelines.

Administration of substances. GDNF enemas (10µl at 1mg/ml in PBS) were administered once daily between P4 to P8, using a 24-gauge gavage needle (Fine Science Tools, Canada) connected to a micropipette, as previously described [19,20]. Briefly, the tip of the gavage needle was gently inserted into the rectum just beyond the anus, and the enema was carefully injected over a few seconds. Two different batches of human recombinant GDNF were used, both standardly produced in bacteria. Research-grade GDNF purchased from PeproTech (cat. #450-10, Cranbury, NJ) was used for single-cell RNA-seq experiments, while clinical-grade GDNF kindly provided by Vivifi Biotech (London, United-Kingdom) was used for all other experiments. When required, tamoxifen (20µl at 4mg/ml in corn oil; Sigma Cat.#10540-29-1) and/or EdU (10 µl at 10mM in PBS; Thermo Fisher Cat.# C10337) were administered via daily intraperitoneal injections in parallel to GDNF enemas, but starting a day earlier (P3-P8). Phospho-FAK[Y397] and phospho-RET[Y1062] inhibitors, PF-562271 (MedChemExpress Cat.# HY-10459) and Pralsetinib/BLU-667 (MedChemExpress Cat.# HY-112301), respectively, were similarly administered via daily intraperitoneal injections using the same 30mg/kg concentration (in a vehicle solution of 2% DMSO; 25% PEG 300; 5% Tween 80; 68% Saline), but in this case only during the GDNF treatment period (P4-P8).

***Human Tissues*.** Human colon samples were obtained from three patients diagnosed with short-segment HSCR who underwent surgical resection of their aganglionic colon segment. These patients were recruited at the Centre hospitalier universitaire Sainte-Justine in Montreal, Canada, and their ages ranged between 3 to 6 months at the time of surgery. Informed consent for the collection and use of these tissues was obtained from all parents or legal guardian. Following surgical resection, full-thickness colon samples of the aganglionic segment were immediately placed in ice-cold, oxygenated Krebs solution and promptly transported to the research laboratory at UQAM for further processing. The use of human samples in our experiments strictly adhered to the guidelines and approval of the human research ethics committees of the Centre Hospitalier Universitaire Sainte-Justine (CER protocol #4172).

Single-cell RNA-seq. Samples of distal colon (last 1 cm) were dissected from P10 *Hol*$^{Tg/Tg}$*;G4-RFP* double-transgenic pups that were previously administered GDNF enemas or not between P4-P8. For each condition, distal colon samples were collected from 6 to 8 pups and pooled on the day of dissection. Once pooled, each piece of distal colon was cut opened along the longitudinal axis, washed extensively in ice-cold PBS, and mechanically dissociated during 5 minutes using a scalpel blade in a small volume (just sufficient to wet the tissue) of pre-warmed (37°C) EMEM (Eagle's Minimum Essential Medium) containing collagenase (0.4 mg/ml; Sigma-Aldrich C2674), dispase II (1.3 mg/ml; Life Technologies 17105-041), and DNAse I (0.5 mg/ml; Sigma-Aldrich DN25). The resulting grossly dissociated tissue preparation was transferred in an Eppendorf tube, into which the above dissociation medium was added to reach ~1 ml total volume, and the tube was then placed in an agitating heating block at 37°C for 30 minutes at 300rpm. The final tissue preparation was filtered through a 40µm cell strainer and centrifuged at 1200 rpm for 5 minutes at 4°C. Pelleted cells were resuspended in 500 µl of sterile PBS also containing 0.04% non-acetylated BSA, stained with CellTracker™ Green CMFDA Dye (Invitrogen, Cat.#C2925) diluted at 1/10000, and separated in a BD FACSJazz cell sorter (BD Biosciences) to specifically recover viable CMFDA+ RFP+ cells. Single-cell RNA-seq libraries were prepared following the guidelines of the 10× Genomics protocol. Brefly, single-cell Gel Bead-In-Emulsions (GEMs) were generated by combining suspended cells, barcoded gel beads, and master mix onto the Chromium Next GEM Chip G, which was then processed on the Chromium iX controller Instrument. After breaking the GEMs, barcoded cDNAs were purified and amplified according to the desired cell recovery target. Subsequently, the cDNA underwent fragmentation, A-tailing, and ligation with adaptors. For sample indexing, additional PCR cycles were conducted based on cDNA input quantified during the QC step. The resulting libraries were finally subjected to 100bp paired-end sequencing on an Illumina NovaSeq 6000 sequencer.

Single-cell RNA-seq data analysis Single-cell RNA-seq data were analyzed using Trailmaker (Parse Biosciences). After alignment to the reference genome (mm10) and transcript quantification, quality

filtering was applied to exclude low-quality cells. The initial dataset contained 10,018 to 9,477 barcodes, depending on the experimental conditions, with a total of 22,142 to 22,778 detected genes. A mitochondrial content filter was applied, setting a maximum threshold of 10% mitochondrial reads with a bin step of 0.30. After filtering, the number of retained cells decreased from 10,018 to 3,997 in the untreated *Hol*$^{Tg/Tg}$ group (-60.1%) and from 9,477 to 7,091 in the GDNF-treated *Hol*$^{Tg/Tg}$ group (-25.2%). Data normalization and batch effect correction were performed using the integrated Trailmaker tools. Dimensionality reduction was conducted via principal component analysis (PCA), and cell clustering was performed with the Leiden algorithm. Cell populations were visualized using uniform manifold approximation and projection (UMAP). Cluster annotation was performed by comparing differentially expressed marker genes with reference databases (PanglaoDB, CellMarker). Differential gene expression analysis was carried out using the Wilcoxon test implemented in Trailmaker. Cell trajectory reconstruction was conducted using Trailmaker's pseudotime tools.

Tissue processing, labelling and imaging. Mouse colon tissues to be immunostained were cut longitudinally along the mesentery, washed in PBS, pinned onto Sylgard-coated (Thermo Fisher Scientific Cat. #50822180) petri dishes, fixed with 4% PFA at 4°C overnight, and finally further microdissected to separate muscle and mucosa layers. Whole muscle strips of distal colon (last 1 cm) were then used for immunofluorescence staining, which was performed as previously described [19]. For human colon tissues, immunofluorescence staining was performed on full-thickness aganglionic samples using a previously described protocol for 3-dimensional imaging [68]. All antibodies used for immunostaining of mouse and human tissues are listed in Table S2. EdU detection in mouse samples was performed using the Invitrogen Click-iT EdU Imaging Kit (Thermo Fisher Scientific Cat. #C10337), in accordance with the manufacturer's instructions. All images were acquired on a Nikon A1 confocal microscope, using either Plan Fluor 20x/0.75 MImm or Plan Apo λ 60x/1.40 objectives (Nikon A1R, Melville, NY). For each biological replicate, between 3 to 10 representative z-stack images of the myenteric plexus were acquired, and then analyzed using the ImageJ software (National Institutes of Health, Bethesda, MD).

Western blot analysis. Remaining part of colon samples not used for immunofluorescence (*i.e.*, proximal and mid segments) were homogenized in RIPA buffer containing protease and phosphatase inhibitors and subjected to centrifugation (14000rpm for 15min at 4C) to sediment debris. The protein concentration in the supernatant was determined using a DC protein assay (Bio-Rad Kit I #5000111) according to the manufacturer's guidelines. For western blot analysis, 50 µg of total protein extracts were separated on a 10% SDS-PAGE and then transferred onto an Immun-Blot PVDF membrane (Bio-Rad Cat. #1620177). The immunoreactive bands were revealed using Immobilon Western Chemiluminescent HRP Substrate (MilliporeSigma Cat. #WBKLS0050) and visualized using the

Fusion FX imaging system (Vilber, Marne-la-Vallée, France). All antibodies used are detailed in Table S2.

Data statistics. Statistical analyses were performed using GraphPad Prism v9.5.1. As indicated in Figure legends, either Student's *t*-tests or one-way ANOVA with post-hoc Tukey's test were used to calculate statistical significance, with P values < 0.05 considered as indicative of significance. All experiments included a minimum of 3 biological replicates.

ACKNOWLEDGEMENTS

The authors thank Gregoire Bonnamour from the Cellular analyses and Imaging core (CERMO-FC, UQAM) for assistance with flow cytometry and confocal imaging. This study was funded by a grant from the Canadian Institutes of Health Research (CIHR grant # PJT-180290) to NP.

AUTHOR CONTRIBUTION

Conceived and Supervised the study: RS and NP. Designed the experiments: AG, RS and NP. Contributed study materials: AA and CF. Performed the experiments: AG, MAL, NL and RS. Analyzed the data: AG, RS and NP. Wrote the paper: AG (original draft), RS (original draft and review), and NP (review and editing). All authors read and approved the final manuscript.

COMPETING INTERESTS

RS and NP are co-founders of the biotech company Neurenati Therapeutics, which had no role in the design of the study; in the collection, analyses, or interpretation of data; in the writing of the manuscript, or in the decision to publish the results. The remaining authors declare no competing interests.

MATERIALS AND CORRESPONDENCE

Correspondence and materials requests should be addressed to NP.

FIGURE LEGENDS

Figure 1. The distal colon of *Hol$^{Tg/Tg}$;G4-RFP* mice is enriched in SCPs and EGCs.
a. Overview of the experimental procedure, from GDNF treatment regimen to scRNA-seq analysis of FACS-recovered RFP+ cells at P10. **b,c.** Uniform manifold approximation and projection (UMAP) visualization showing unsupervised clustering of SCPs, EGCs and enteric neurons from the distal colon of P10 *Hol$^{Tg/Tg}$;G4-RFP* mice that were previously treated (c) or not (b) with GDNF. **d.** Dot plot showing the relative expression levels of a selection of marker genes in each cluster. **e.** UMAP visualization showing all clusters stratified by experimental group (untreated *vs*. GDNF-treated *Hol$^{Tg/Tg}$;G4-RFP* mice). **f.** Comparative frequency plots showing the relative proportion of each cluster in untreated *vs*. GDNF-treated *Hol$^{Tg/Tg}$;G4-RFP* mice.

Figure 2. The neurogenic effect of GDNF in *Hol$^{Tg/Tg}$;G4-RFP* mice is mediated by NCAM1, not RET.
a. Feature plots showing the relative gene expression levels of signaling (*Ret* and *Ncam1*) and binding (*Gfra1, Gfra2, Gfra3, Gfra4*) GDNF receptors in the scRNA-seq dataset of GDNF-treated *Hol$^{Tg/Tg}$;G4-RFP* mice. **b.** Immunofluorescence staining of NCAM1 and its downstream signaling effector phospho-FAK[Y397] in the distal colon of *Hol$^{Tg/Tg}$* mice at the indicated time points before, during and after GDNF treatment (representative images of N=3 animals per time point). **c.** Immunofluorescence staining of HuC/D and SOX10 in the distal colon of P8 *Hol$^{Tg/Tg}$* mice that were administered GDNF enemas and were also injected with selective inhibitors (or vehicle only) for phospho-FAK[Y397] (PF-562271) or phosphoRET[Y1062] (BLU-667) from P4 onwards. Quantitative analysis of the number of HuC/D+ neurons per mm^2 is shown on the right, with each value corresponding to a microscopic field of view (7 to 10 fields of view per animal; N indicates the number of animals per group; n indicates the total number of counted cells). ****$P < 0.0001$; Ordinary one-way ANOVA with post-hoc Tukey's test. The dashed outlines in panels b-c highlight either extrinsic nerve fibers or an individual ganglion. Scale bar, 25 µm (b) and 150 µm (c).

Figure 3. Re-clustering based on *Elavl4* expression reveals a stepwise differentiation mechanism connecting SCPs, EGCs and enteric neurons.
a. Feature plot showing the relative expression levels of the neuronal marker gene *Elavl4* in the scRNA-seq dataset of GDNF-treated *Hol$^{Tg/Tg}$;G4-RFP* mice. **b.** UMAP visualization of the scRNA-seq dataset of GDNF-treated *Hol$^{Tg/Tg}$;G4-RFP* mice after reclustering based on *Elavl4* expression levels. **c.** Dot plot showing the relative expression levels of a selection of marker genes in each cluster. **d.** Feature plots showing the relative gene expression levels of pan-glial (*Sox10*), pan-neuronal (*Elavl4* and *Tubb3*), SCP (*Mpz* and *Dhh*), cycling cell (*Ubec2c*) and EGC (*Gfap* and *Slc18a2*) markers. **e.** Pseudotime analysis of *Elavl4*-based reclustered scRNA-seq datasets of untreated and GDNF-treated *Hol$^{Tg/Tg}$;G4-RFP* mice.

Figure 4. GDNF-induced neuronal differentiation of SCPs occurs in part via and EGC-like state.
a,b. Immunofluorescence staining of P10 distal colon samples from GDNF-treated *Hol$^{Tg/Tg}$;Dhh-Cre$^{Tg/+}$;R26$^{YFP/+}$* mice showing several newly induced myenteric ganglion cells derived from SCPs (YFP+) that are undergoing neuronal differentiation (PHOX2B+) while also expressing either GFAP (a) or SLC18A2 (b) EGC markers (see yellow arrows; representative images of N=3 animals). **c.** Immunofluorescence staining of distal colon samples from GDNF-treated *Hol$^{Tg/Tg;}$Dhh-Cre$^{Tg/+}$;R26$^{YFP/+}$* mice at indicated time points showing that the proportion of SCP-derived (YFP+) myenteric ganglion cells also positive for the EGC marker GFAP decreases over time. Yellow and white arrows point to GFAP+ cells that are either YFP+ or YFP-, respectively. Quantitative analysis of the percentage of double YFP+ GFAP+ myenteric ganglion cells is shown on the right, with each value corresponding to a microscopic field of view (7 to 10 fields of view per animal; N indicates the number of animals per group; n indicates the total number of counted cells). ****$P < 0.0001$; Ordinary one-way ANOVA with

post-hoc Tukey's test. The dashed outlines in panels a-c highlight an individual ganglion. Scale bar, 25 µm.

Figure 5. GDNF-induced neurogenesis is more rapid from SCPs than from EGCs.
a. Diagram of the time-course experimental procedure and involved mouse models for comparative genetic cell lineage tracing in the *Hol*$^{Tg/Tg}$ mutant background. **b.** Quantitative analysis of the density of GDNF-induced myenteric neurons in the distal colon of *Hol*$^{Tg/Tg}$ mice as a function of time, regardless of cell lineage tracing tools. Each value corresponds to a microscopic field of view (7 to 10 fields of view per animal; N indicates the number of animals; n indicates the total number of counted cells). ****$P < 0.0001$; ordinary one-way ANOVA with post-hoc Tukey's test. **c-e.** Immunofluorescence-based kinetic analysis of distal colon myenteric SOX10+ glia (yellow arrows) or HuC/D+ neurons (yellow arrowheads) that are also positive for YFP, which indicates whether they are derived from *Dhh*-expressing SCPs (c), *Slc18a2*-expressing EGCs (d) or *Gfap*-expressing EGCs (e). Each value in the accompanying quantitative analyses corresponds to a microscopic field of view (7 to 11 fields of view per animal; N indicates the number of animals; n indicates the total number of counted cells). *$P < 0.5$; ***$P < 0.001$; ****$P < 0.0001$; ordinary one-way ANOVA with post-hoc Tukey's test. The dashed outlines in panels c-e highlight an individual ganglion. Scale bar, 25 µm.

Figure 6. GDNF predominantly promotes the direct transdifferentiation of ENS progenitors into neurons.
a. Diagram of the time-course experimental procedure and involved mouse models for combined EdU incorporation assays and genetic cell lineage tracing in the *Hol*$^{Tg/Tg}$ mutant background. **b.** Quantitative analysis of the percentage of GDNF-induced HuC/D+ myenteric neurons that did not incorporate EdU in the distal colon of *Hol*$^{Tg/Tg}$ mice as a function of time, regardless of cell lineage tracing tools. Each value corresponds to a microscopic field of view (7 to 11 fields of view per animal; N indicates the number of animals; n indicates the total number of counted cells). ***$P < 0.001$; ****$P < 0.0001$; ordinary one-way ANOVA with post-hoc Tukey's test. **c-e**. Immunofluorescence-based kinetic analysis of distal colon myenteric HuC/D+ neurons (yellow arrowheads) that have incorporated EdU and are also positive for YFP, which indicates whether they are derived from *Dhh*-expressing SCPs (c), *Slc18a2*-expressing EGCs (d) or *Gfap*-expressing EGCs (e). Each value in the accompanying quantitative analyses corresponds to a microscopic field of view (8 to 11 fields of view per animal; N indicates the number of animals; n indicates the total number of counted cells). *$P < 0.05$, **$P < 0.01$, ***$P < 0.001$, ****$P < 0.0001$; ordinary one-way ANOVA with post-hoc Tukey's test (c, d) or unpaired two-tailed Student's *t*-test (e). The dashed outlines in panels c-e highlight an individual ganglion. Scale bar, 20 µm.

Figure 7. A neural crest-independent subtype of ENS progenitors is required for balancing cholinergic *vs*. nitrergic differentiation of GDNF-induced myenteric neurons.
a,b. Immunofluorescence-based analysis of the relative proportions of nitrergic (NOS1+) and cholinergic (ChAT+) neurons among GDNF-induced myenteric neurons (HuC/D+) at P20, with YFP signal (yellow arrowheads) further indicative of their origin from *Dhh*-expressing SCPs (a) or *Gfap*-expressing EGCs (b). Each value in the accompanying quantitative analyses corresponds to a microscopic field of view (8 to 11 fields of view per animal; N indicates the number of animals; n indicates the total number of counted cells). **c.** Immunofluorescence-based analysis of the contribution of *Wnt1*-expressing NCCs (YFP+) to the overall pool of HuC/D+ neurons and SOX10+ EGCs in the distal colon of P20 WT-like control and GDNF-treated *Hol*$^{Tg/Tg}$ mutant mice. Empty arrowheads point to YFP-negative neurons in the *Hol*$^{Tg/Tg}$ mutant background. Each value in the accompanying quantitative analyses corresponds to a microscopic field of view (7 to 11 fields of view per animal; N indicates the number of animals; n indicates the total number of counted cells). **d.** Immunofluorescence-based analysis of the relative proportions of nitrergic (NOS1+) and cholinergic (ChAT+) neurons among GDNF-induced myenteric neurons (HuC/D+) at P20, with YFP signal further indicative of their origin from *Wnt1*-expressing NCCs. Empty arrowheads point to YFP-negative neurons. Each value in the accompanying quantitative analysis corresponds to a microscopic field of view (7 to 8 fields of view

per animal; N indicates the number of animals; n indicates the total number of counted cells). ****P < 0.0001; unpaired two-tailed Student's *t*-test. The dashed outlines highlight an individual ganglion. Scale bar, 25 µm**.**

Figure 8. Graphical summary of the main findings of this study.
Rectal administration of GDNF to *Hol*$^{Tg/Tg}$ pups during only 5 days triggers rapid enteric neurogenesis that persists beyond the treatment period. This neurogenic effect of GDNF is mediated by the NCAM1/FAK signaling axis, which must be activated in various subtypes of ENS progenitors with complementary differentiation potential. These tissue-resident progenitors include neural crest-derived SCPs and EGCs, as well as an enigmatic non-neural crest-derived subtype.

REFERENCES

1 Furness, J. B. The enteric nervous system and neurogastroenterology. *Nat Rev Gastroenterol Hepatol* **9**, 286-294 (2012). https://doi.org/nrgastro.2012.32 [pii]10.1038/nrgastro.2012.32

2 Schneider, S., Wright, C. M. & Heuckeroth, R. O. Unexpected Roles for the Second Brain: Enteric Nervous System as Master Regulator of Bowel Function. *Annu Rev Physiol* **81**, 235-259 (2019). https://doi.org/10.1146/annurev-physiol-021317-121515

3 Rao, M. & Gershon, M. D. The bowel and beyond: the enteric nervous system in neurological disorders. *Nat Rev Gastroenterol Hepatol* **13**, 517-528 (2016). https://doi.org/10.1038/nrgastro.2016.107

4 Lefevre, M. A., Soret, R. & Pilon, N. Harnessing the Power of Enteric Glial Cells' Plasticity and Multipotency for Advancing Regenerative Medicine. *Int J Mol Sci* **24** (2023). https://doi.org/10.3390/ijms241512475

5 Pilon, N. Treatment and Prevention of Neurocristopathies. *Trends in molecular medicine* **27**, 451-468 (2021). https://doi.org/10.1016/j.molmed.2021.01.009

6 Kapur, R. P., Yost, C. & Palmiter, R. D. A transgenic model for studying development of the enteric nervous system in normal and aganglionic mice. *Development* **116**, 167-175 (1992). https://doi.org/10.1242/dev.116.Supplement.167

7 Yntema, C. L. & Hammond, W. S. The origin of intrinsic ganglia of trunk viscera from vagal neural crest in the chick embryo. *J Comp Neurol* **101**, 515-541 (1954).

8 Bergeron, K. F., Silversides, D. W. & Pilon, N. The developmental genetics of Hirschsprung's disease. *Clin Genet* **83**, 15-22 (2013). https://doi.org/10.1111/cge.12032

9 Heuckeroth, R. O. Hirschsprung disease - integrating basic science and clinical medicine to improve outcomes. *Nat Rev Gastroenterol Hepatol* **15**, 152-167 (2018). https://doi.org/10.1038/nrgastro.2017.149

10 Uesaka, T., Nagashimada, M. & Enomoto, H. Neuronal Differentiation in Schwann Cell Lineage Underlies Postnatal Neurogenesis in the Enteric Nervous System. *J Neurosci* **35**, 9879-9888 (2015). https://doi.org/10.1523/JNEUROSCI.1239-15.2015

11 Lefevre, M. A., Godefroid, Z., Soret, R. & Pilon, N. Enteric glial cell diversification is influenced by spatiotemporal factors and source of neural progenitors in mice. *Front Neurosci* **18**, 1392703 (2024). https://doi.org/10.3389/fnins.2024.1392703

12 Watanabe, Y. *et al.* Morphological investigation of the enteric nervous system in Hirschsprung's disease and hypoganglionosis using whole-mount colon preparation. *J Pediatr Surg* **34**, 445-449 (1999).

13 Uesaka, T. *et al.* Enhanced enteric neurogenesis by Schwann cell precursors in mouse models of Hirschsprung disease. *Glia* (2021). https://doi.org/10.1002/glia.24059

14 Rialon, K. L. & Langer, J. C. Pullthrough pitfalls in treating Hirschsprung disease. *World J Pediatr Surg* **7**, e000862 (2024). https://doi.org/10.1136/wjps-2024-000862

15 Swenson, O. & Bill, A. H., Jr. Resection of rectum and rectosigmoid with preservation of the sphincter for benign spastic lesions producing megacolon; an experimental study. *Surgery* **24**, 212-220 (1948).

16 Dariel, A. *et al.* Analysis of enteric nervous system and intestinal epithelial barrier to predict complications in Hirschsprung's disease. *Scientific reports* **10**, 21725 (2020). https://doi.org/10.1038/s41598-020-78340-z

17 Rintala, R. J. & Pakarinen, M. P. Long-term outcomes of Hirschsprung's disease. *Semin Pediatr Surg* **21**, 336-343 (2012). https://doi.org/10.1053/j.sempedsurg.2012.07.008

18 Quiroz, H. J. *et al.* Pull-through procedure in children with Hirschsprung disease: A nationwide analysis on postoperative outcomes. *J Pediatr Surg* **55**, 899-903 (2020). https://doi.org/10.1016/j.jpedsurg.2020.01.038

19 Soret, R. *et al.* Glial Cell Derived Neurotrophic Factor Induces Enteric Neurogenesis and Improves Colon Structure and Function in Mouse Models of Hirschsprung Disease. *Gastroenterology* **159**, 1824-1838.e1817 (2020). https://doi.org/10.1053/j.gastro.2020.07.018

20 Soret, R. *et al.* Genetic Background Influences Severity of Colonic Aganglionosis and Response to GDNF Enemas in the Holstein Mouse Model of Hirschsprung Disease. *Int J Mol Sci* **22** (2021). https://doi.org/10.3390/ijms222313140

21 Durbec, P. *et al.* GDNF signalling through the Ret receptor tyrosine kinase. *Nature* **381**, 789-793 (1996). https://doi.org/10.1038/381789a0

22 Mwizerwa, O. *et al.* Gdnf is mitogenic, neurotrophic, and chemoattractive to enteric neural crest cells in the embryonic colon. *Dev Dyn* **240**, 1402-1411 (2011). https://doi.org/10.1002/dvdy.22630

23 Young, H. M. *et al.* GDNF is a chemoattractant for enteric neural cells. *Dev Biol* **229**, 503-516 (2001).

24 Uesaka, T., Nagashimada, M. & Enomoto, H. GDNF signaling levels control migration and neuronal differentiation of enteric ganglion precursors. *J Neurosci* **33**, 16372-16382 (2013). https://doi.org/10.1523/JNEUROSCI.2079-13.2013

25 Heuckeroth, R. O. Hirschsprung disease - integrating basic science and clinical medicine to improve outcomes. *Nature reviews. Gastroenterology & hepatology* (2018). https://doi.org/10.1038/nrgastro.2017.149

26 Montalva, L. *et al.* Hirschsprung disease. *Nat Rev Dis Primers* **9**, 54 (2023). https://doi.org/10.1038/s41572-023-00465-y

27 Tilghman, J. M. *et al.* Molecular Genetic Anatomy and Risk Profile of Hirschsprung's Disease. *N Engl J Med* **380**, 1421-1432 (2019). https://doi.org/10.1056/NEJMoa1706594

28 Virtanen, V. B. *et al.* Noncoding RET variants explain the strong association with Hirschsprung disease in patients without rare coding sequence variant. *European journal of medical genetics* **62**, 229-234 (2019). https://doi.org/10.1016/j.ejmg.2018.07.019

29 Paratcha, G., Ledda, F. & Ibanez, C. F. The neural cell adhesion molecule NCAM is an alternative signaling receptor for GDNF family ligands. *Cell* **113**, 867-879 (2003).

30 Sjostrand, D. & Ibanez, C. F. Insights into GFRalpha1 regulation of neural cell adhesion molecule (NCAM) function from structure-function analysis of the NCAM/GFRalpha1 receptor complex. *J Biol Chem* **283**, 13792-13798 (2008). https://doi.org/10.1074/jbc.M800283200

31 Pilon, N. Pigmentation-based insertional mutagenesis is a simple and potent screening approach for identifying neurocristopathy-associated genes in mice. *Rare Diseases* **4**, e1156287 (2016).

32 Soret, R. *et al.* A collagen VI-dependent pathogenic mechanism for Hirschsprung's disease. *J Clin Invest* **125**, 4483-4496 (2015). https://doi.org/10.1172/JCI83178

33 Heuckeroth, R. O. Hirschsprung's disease, Down syndrome, and missing heritability: too much collagen slows migration. *J Clin Invest* **125**, 4323-4326 (2015). https://doi.org/10.1172/JCI85003

34 Bergeron, K. F. *et al.* Male-Biased Aganglionic Megacolon in the TashT Mouse Line Due to Perturbation of Silencer Elements in a Large Gene Desert of Chromosome 10. *PLoS Genet* **11**, e1005093 (2015). https://doi.org/10.1371/journal.pgen.1005093

35 Hosoda, K. *et al.* Targeted and natural (piebald-lethal) mutations of endothelin-B receptor gene produce megacolon associated with spotted coat color in mice. *Cell* **79**, 1267-1276 (1994). https://doi.org/0092-8674(94)90017-5 [pii]

36 Pilon, N., Raiwet, D., Viger, R. S. & Silversides, D. W. Novel pre- and post-gastrulation expression of Gata4 within cells of the inner cell mass and migratory neural crest cells. *Dev Dyn* **237**, 1133-1143 (2008).

37 Bergeron, K. F. *et al.* Upregulation of the Nr2f1-A830082K12Rik gene pair in murine neural crest cells results in a complex phenotype reminiscent of waardenburg syndrome type 4. *Disease models & mechanisms* **9**, 1283-1293 (2016). https://doi.org/10.1242/dmm.026773

38 Sariola, H. & Saarma, M. Novel functions and signalling pathways for GDNF. *Journal of cell science* **116**, 3855-3862 (2003). https://doi.org/10.1242/jcs.00786

39 Roberts, W. G. *et al.* Antitumor activity and pharmacology of a selective focal adhesion kinase inhibitor, PF-562,271. *Cancer Res* **68**, 1935-1944 (2008). https://doi.org/10.1158/0008-5472.CAN-07-5155

40 Subbiah, V. *et al.* Precision Targeted Therapy with BLU-667 for RET-Driven Cancers. *Cancer Discov* **8**, 836-849 (2018). https://doi.org/10.1158/2159-8290.CD-18-0338

41 Tumer, N. *et al.* Hypothalamic rAAV-mediated GDNF gene delivery ameliorates age-related obesity. *Neurobiol Aging* **27**, 459-470 (2006). https://doi.org/10.1016/j.neurobiolaging.2005.03.018

42 Belkind-Gerson, J. *et al.* Colitis promotes neuronal differentiation of Sox2+ and PLP1+ enteric cells. *Scientific reports* **7**, 2525 (2017). https://doi.org/10.1038/s41598-017-02890-y

43 Joseph, N. M. *et al.* Enteric glia are multipotent in culture but primarily form glia in the adult rodent gut. *J Clin Invest* **121**, 3398-3411 (2011). https://doi.org/58186 [pii]10.1172/JCI58186

44 Laranjeira, C. *et al.* Glial cells in the mouse enteric nervous system can undergo neurogenesis in response to injury. *J Clin Invest* **121**, 3412-3424 (2011). https://doi.org/58200 [pii]10.1172/JCI58200

45 McCallum, S. *et al.* Enteric glia as a source of neural progenitors in adult zebrafish. *Elife* **9** (2020). https://doi.org/10.7554/eLife.56086

46 Mueller, J. L. *et al.* Highly neurogenic glia from human and mouse myenteric ganglia generate functional neurons following culture and transplantation into the gut. *Cell reports* **43**, 114919 (2024). https://doi.org/10.1016/j.celrep.2024.114919

47 Trapnell, C. *et al.* The dynamics and regulators of cell fate decisions are revealed by pseudotemporal ordering of single cells. *Nat Biotechnol* **32**, 381-386 (2014). https://doi.org/10.1038/nbt.2859

48 Guyer, R. A. *et al.* Single-cell multiome sequencing clarifies enteric glial diversity and identifies an intraganglionic population poised for neurogenesis. *Cell reports* **42**, 112194 (2023). https://doi.org/10.1016/j.celrep.2023.112194

49 Windster, J. D. *et al.* Human Enteric Glia Diversity in Health and Disease: New Avenues for the Treatment of Hirschsprung Disease. *Gastroenterology* (2024). https://doi.org/10.1053/j.gastro.2024.12.011

50 Jaegle, M. *et al.* The POU proteins Brn-2 and Oct-6 share important functions in Schwann cell development. *Genes Dev* **17**, 1380-1391 (2003). https://doi.org/10.1101/gad.258203

51 Srinivas, S. *et al.* Cre reporter strains produced by targeted insertion of EYFP and ECFP into the ROSA26 locus. *BMC Dev Biol* **1**, 4 (2001).

52 Ganat, Y. M. *et al.* Early postnatal astroglial cells produce multilineage precursors and neural stem cells in vivo. *J Neurosci* **26**, 8609-8621 (2006). https://doi.org/10.1523/JNEUROSCI.2532-06.2006

53 Gerfen, C. R., Paletzki, R. & Heintz, N. GENSAT BAC cre-recombinase driver lines to study the functional organization of cerebral cortical and basal ganglia circuits. *Neuron* **80**, 1368-1383 (2013). https://doi.org/10.1016/j.neuron.2013.10.016

54 Lewis, A. E., Vasudevan, H. N., O'Neill, A. K., Soriano, P. & Bush, J. O. The widely used Wnt1-Cre transgene causes developmental phenotypes by ectopic activation of Wnt signaling. *Dev Biol* **379**, 229-234 (2013). https://doi.org/10.1016/j.ydbio.2013.04.026

55 Moore, M. W. *et al.* Renal and neuronal abnormalities in mice lacking GDNF. *Nature* **382**, 76-79 (1996). https://doi.org/10.1038/382076a0

56 Schuchardt, A., D'Agati, V., Larsson-Blomberg, L., Costantini, F. & Pachnis, V. Defects in the kidney and enteric nervous system of mice lacking the tyrosine kinase receptor Ret. *Nature* **367**, 380-383 (1994). https://doi.org/10.1038/367380a0

57 Gui, H. *et al.* Whole exome sequencing coupled with unbiased functional analysis reveals new Hirschsprung disease genes. *Genome Biol* **18**, 48 (2017). https://doi.org/10.1186/s13059-017-1174-6

58 Tang, C. S. *et al.* Identification of Genes Associated With Hirschsprung Disease, Based on Whole-Genome Sequence Analysis, and Potential Effects on Enteric Nervous System Development. *Gastroenterology* **155**, 1908-1922 e1905 (2018). https://doi.org/10.1053/j.gastro.2018.09.012

59 Gianino, S., Grider, J. R., Cresswell, J., Enomoto, H. & Heuckeroth, R. O. GDNF availability determines enteric neuron number by controlling precursor proliferation. *Development* **130**, 2187-2198 (2003).

60 Lake, J. I., Tusheva, O. A., Graham, B. L. & Heuckeroth, R. O. Hirschsprung-like disease is exacerbated by reduced de novo GMP synthesis. *J Clin Invest* **123**, 4875-4887 (2013). https://doi.org/10.1172/JCI69781

61 Faure, C. *et al.* Gangliogenesis in the enteric nervous system: roles of the polysialylation of the neural cell adhesion molecule and its regulation by bone morphogenetic protein-4. *Dev Dyn* **236**, 44-59 (2007). https://doi.org/10.1002/dvdy.20943

62 Windster, J. D. *et al.* A combinatorial panel for flow cytometry-based isolation of enteric nervous system cells from human intestine. *EMBO Rep* **24**, e55789 (2023). https://doi.org/10.15252/embr.202255789

63 Shepherd, A. *et al.* RET Signaling Persists in the Adult Intestine and Stimulates Motility by Limiting PYY Release From Enteroendocrine Cells. *Gastroenterology* **166**, 437-449 (2024). https://doi.org/10.1053/j.gastro.2023.11.020

64 Meir, M. *et al.* Neurotrophic factor GDNF regulates intestinal barrier function in inflammatory bowel disease. *J Clin Invest* **129**, 2824-2840 (2019). https://doi.org/10.1172/JCI120261

65 Badizadegan, K. *et al.* Presence of intramucosal neuroglial cells in normal and aganglionic human colon. *American journal of physiology. Gastrointestinal and liver physiology* **307**, G1002-1012 (2014). https://doi.org/10.1152/ajpgi.00164.2014

66 Wilkinson, D. J., Bethell, G. S., Shukla, R., Kenny, S. E. & Edgar, D. H. Isolation of Enteric Nervous System Progenitor Cells from the Aganglionic Gut of Patients with Hirschsprung's Disease. *PLoS One* **10**, e0125724 (2015). https://doi.org/10.1371/journal.pone.0125724

67 Postat, J. & Bousso, P. Quorum Sensing by Monocyte-Derived Populations. *Front Immunol* **10**, 2140 (2019). https://doi.org/10.3389/fimmu.2019.02140

68 Graham, K. D. *et al.* Robust, 3-Dimensional Visualization of Human Colon Enteric Nervous System Without Tissue Sectioning. *Gastroenterology* **158**, 2221-2235 e2225 (2020). https://doi.org/10.1053/j.gastro.2020.02.035

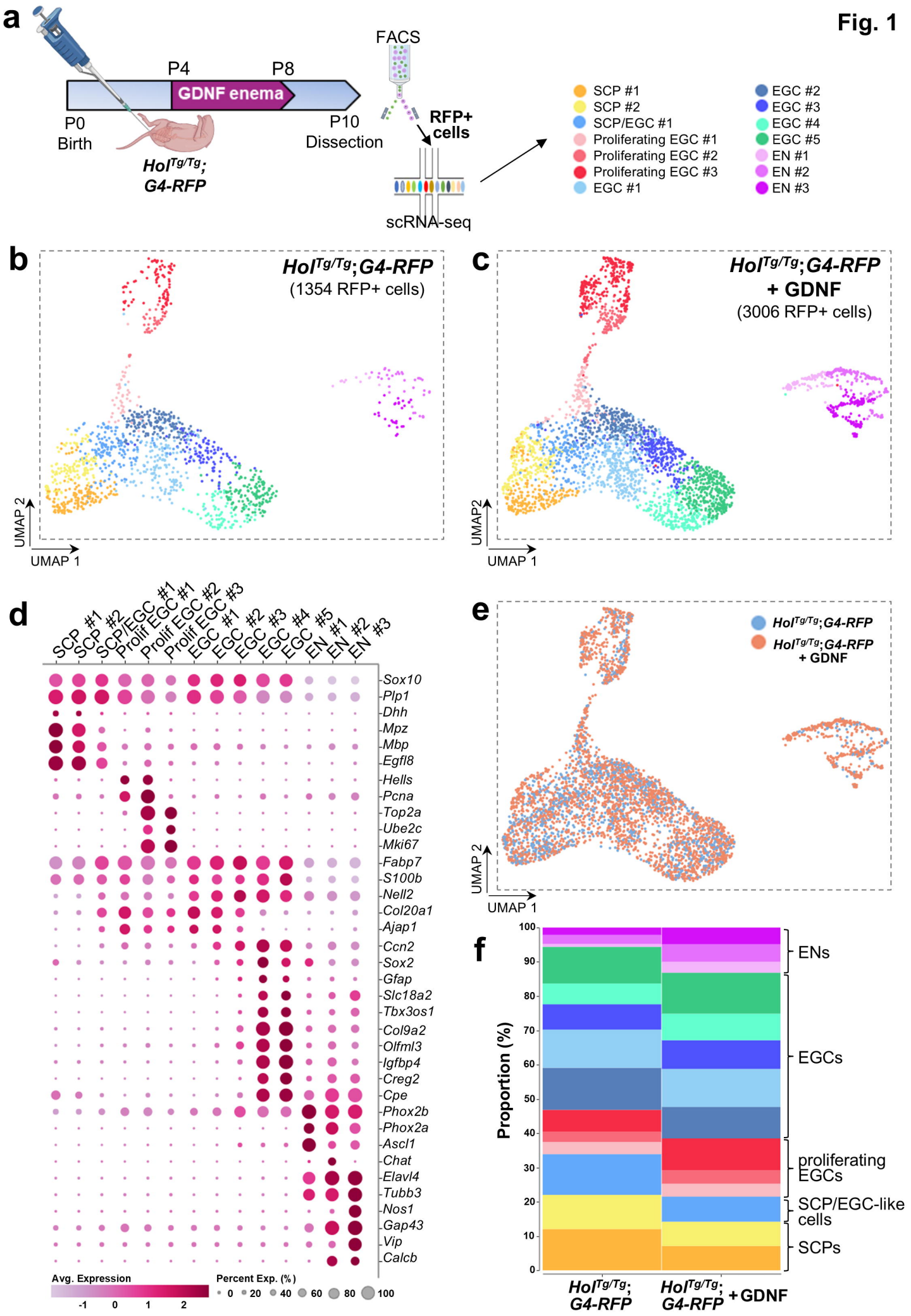
Fig. 1
a
P4
P8
GDNF enema
P0
Birth
P10
Dissection
Hol^Tg/Tg; G4-RFP
FACS
RFP+ cells
scRNA-seq
SCP #1
SCP #2
SCP/EGC #1
Proliferating EGC #1
Proliferating EGC #2
Proliferating EGC #3
EGC #1
EGC #2
EGC #3
EGC #4
EGC #5
EN #1
EN #2
EN #3
b
Hol^Tg/Tg;G4-RFP
(1354 RFP+ cells)
UMAP 2
UMAP 1
c
Hol^Tg/Tg;G4-RFP
+ GDNF
(3006 RFP+ cells)
UMAP2
UMAP 1
d
SCP #1
SCP #2
SCP/EGC #1
Prolif EGC #1
Prolif EGC #1
Prolif EGC #2
Prolif EGC #3
EGC #1
EGC #2
EGC #3
EGC #4
EGC #5
EN #1
EN #2
EN #3
Sox10
Plp1
Dhh
Mpz
Mbp
Egfl8
Hells
Pcna
Top2a
Ube2c
Mki67
Fabp7
S100b
Nell2
Col20a1
Ajap1
Ccn2
Sox2
Gfap
Slc18a2
Tbx3os1
Col9a2
Olfml3
Igfbp4
Creg2
Cpe
Phox2b
Phox2a
Ascl1
Chat
Elavl4
Tubb3
Nos1
Gap43
Vip
Calcb
Avg. Expression
-1
0
1
2
Percent Exp. (%)
0
20
40
60
80
100
e
Hol^Tg/Tg;G4-RFP
Hol^Tg/Tg;G4-RFP
+ GDNF
UMAP 2
UMAP 1
f
Proportion (%)
100
90
80
70
60
50
40
30
20
10
0
ENs
EGCs
proliferating EGCs
SCP/EGC-like cells
SCPs
Hol^Tg/Tg; G4-RFP
Hol^Tg/Tg; G4-RFP +GDNF

Fig. 2

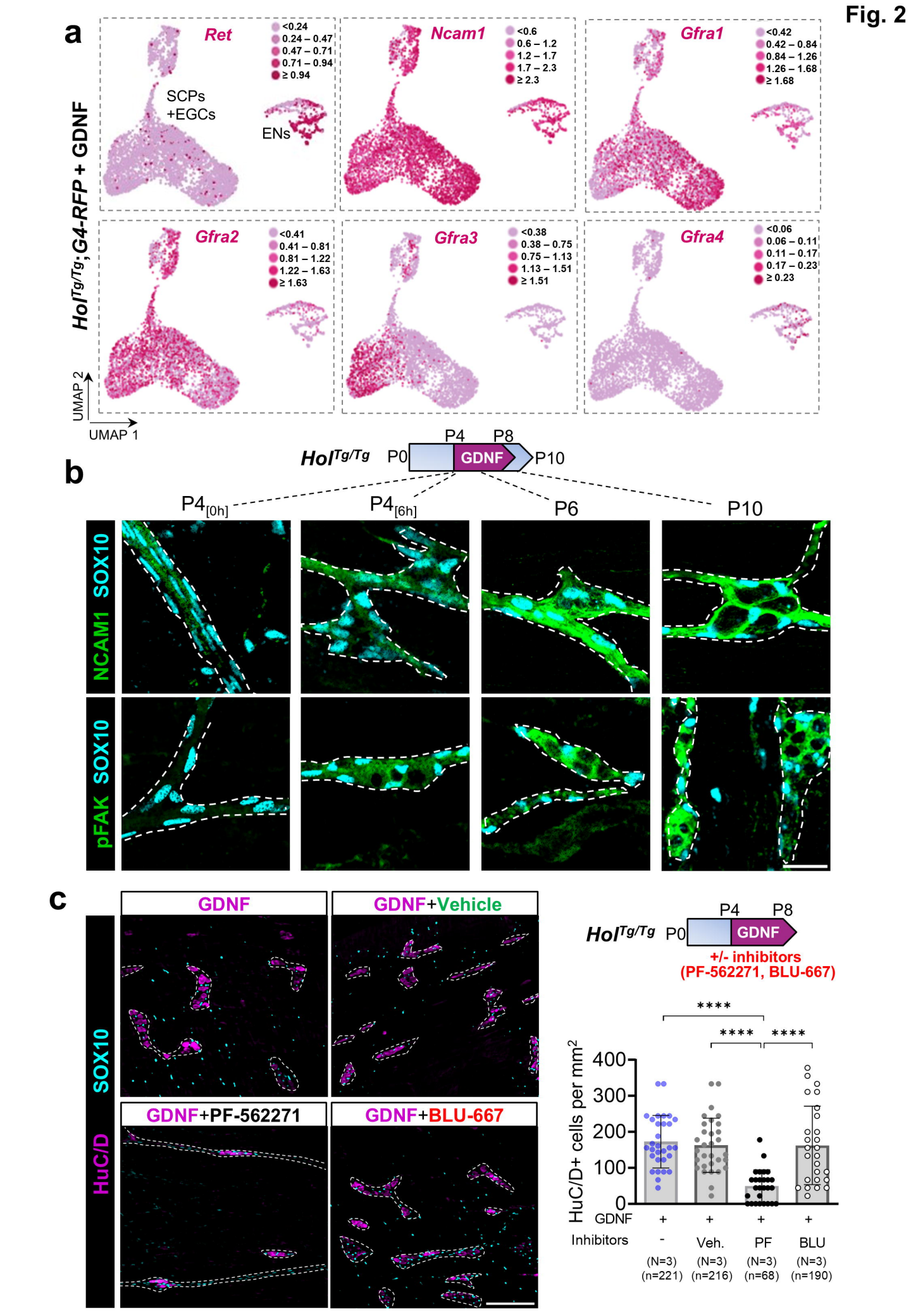
a
Hol Tg/Tg;G4-RFP + GDNF
Ret
<0.24
0.24 – 0.47
0.47 – 0.71
0.71 – 0.94
≥ 0.94
SCPs
+EGCs
ENs
Ncam1
<0.6
0.6 – 1.2
1.2 – 1.7
1.7 – 2.3
≥ 2.3
Gfra1
<0.42
0.42 – 0.84
0.84 – 1.26
1.26 – 1.68
≥ 1.68
Gfra2
<0.41
0.41 – 0.81
0.81 – 1.22
1.22 – 1.63
≥ 1.63
Gfra3
<0.38
0.38 – 0.75
0.75 – 1.13
1.13 – 1.51
≥ 1.51
Gfra4
<0.06
0.06 – 0.11
0.11 – 0.17
0.17 – 0.23
≥ 0.23
UMAP 2
UMAP 1
b
Hol Tg/Tg
P0
P4
P8
GDNF
P10
P4[0h]
P4[6h]
P6
P10
NCAM1 SOX10
pFAK SOX10
c
GDNF
GDNF+Vehicle
GDNF+PF-562271
GDNF+BLU-667
SOX10
HuC/D
Hol Tg/Tg
P0
P4
P8
GDNF
+/- inhibitors
(PF-562271, BLU-667)
****
****
****
HuC/D+ cells per mm2
400
300
200
100
0
GDNF + + + +
Inhibitors - Veh. PF BLU
(N=3) (n=221)
(N=3) (n=216)
(N=3) (n=68)
(N=3) (n=190)

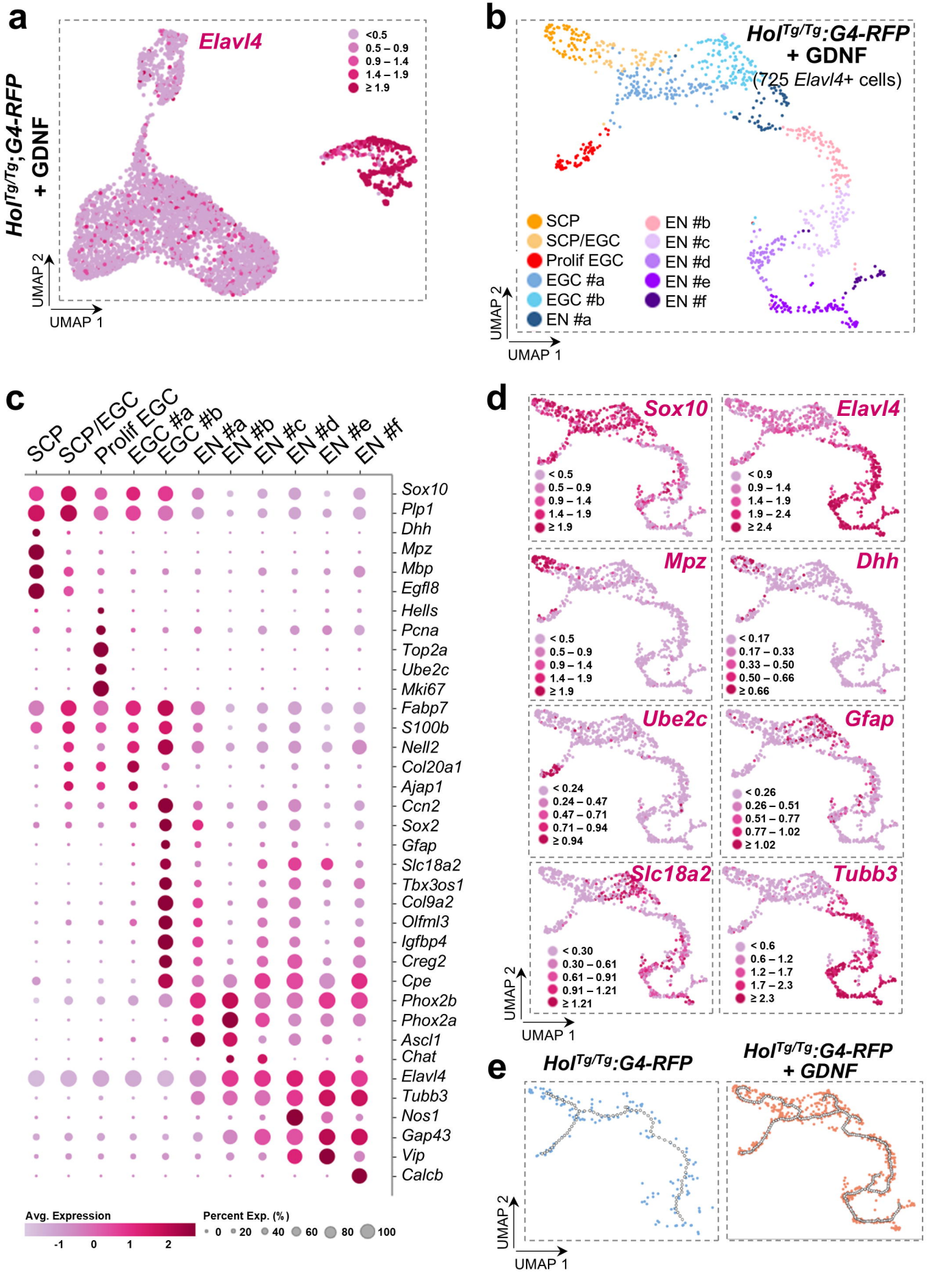
a
Elavl4
<0.5
0.5 – 0.9
0.9 – 1.4
1.4 – 1.9
≥ 1.9
Hol^Tg/Tg;G4-RFP + GDNF
UMAP 2
UMAP 1
b
Hol^Tg/Tg:G4-RFP + GDNF
(725 Elavl4+ cells)
SCP
SCP/EGC
Prolif EGC
EGC #a
EGC #b
EN #a
EN #b
EN #c
EN #d
EN #e
EN #f
UMAP 2
UMAP 1
c
SCP
SCP/EGC
Prolif EGC
EGC #a
EGC #b
EN #a
EN #b
EN #c
EN #d
EN #e
EN #f
Sox10
Plp1
Dhh
Mpz
Mbp
Egfl8
Hells
Pcna
Top2a
Ube2c
Mki67
Fabp7
S100b
Nell2
Col20a1
Ajap1
Ccn2
Sox2
Gfap
Slc18a2
Tbx3os1
Col9a2
Olfml3
Igfbp4
Creg2
Cpe
Phox2b
Phox2a
Ascl1
Chat
Elavl4
Tubb3
Nos1
Gap43
Vip
Calcb
Avg. Expression
-1
0
1
2
Percent Exp. (%)
0
20
40
60
80
100
d
Sox10
< 0.5
0.5 – 0.9
0.9 – 1.4
1.4 – 1.9
≥ 1.9
Elavl4
< 0.9
0.9 – 1.4
1.4 – 1.9
1.9 – 2.4
≥ 2.4
Mpz
< 0.5
0.5 – 0.9
0.9 – 1.4
1.4 – 1.9
≥ 1.9
Dhh
< 0.17
0.17 – 0.33
0.33 – 0.50
0.50 – 0.66
≥ 0.66
Ube2c
< 0.24
0.24 – 0.47
0.47 – 0.71
0.71 – 0.94
≥ 0.94
Gfap
< 0.26
0.26 – 0.51
0.51 – 0.77
0.77 – 1.02
≥ 1.02
Slc18a2
< 0.30
0.30 – 0.61
0.61 – 0.91
0.91 – 1.21
≥ 1.21
Tubb3
< 0.6
0.6 – 1.2
1.2 – 1.7
1.7 – 2.3
≥ 2.3
UMAP 2
UMAP 1
e
Hol^Tg/Tg:G4-RFP
Hol^Tg/Tg:G4-RFP + GDNF
UMAP 2
UMAP 1

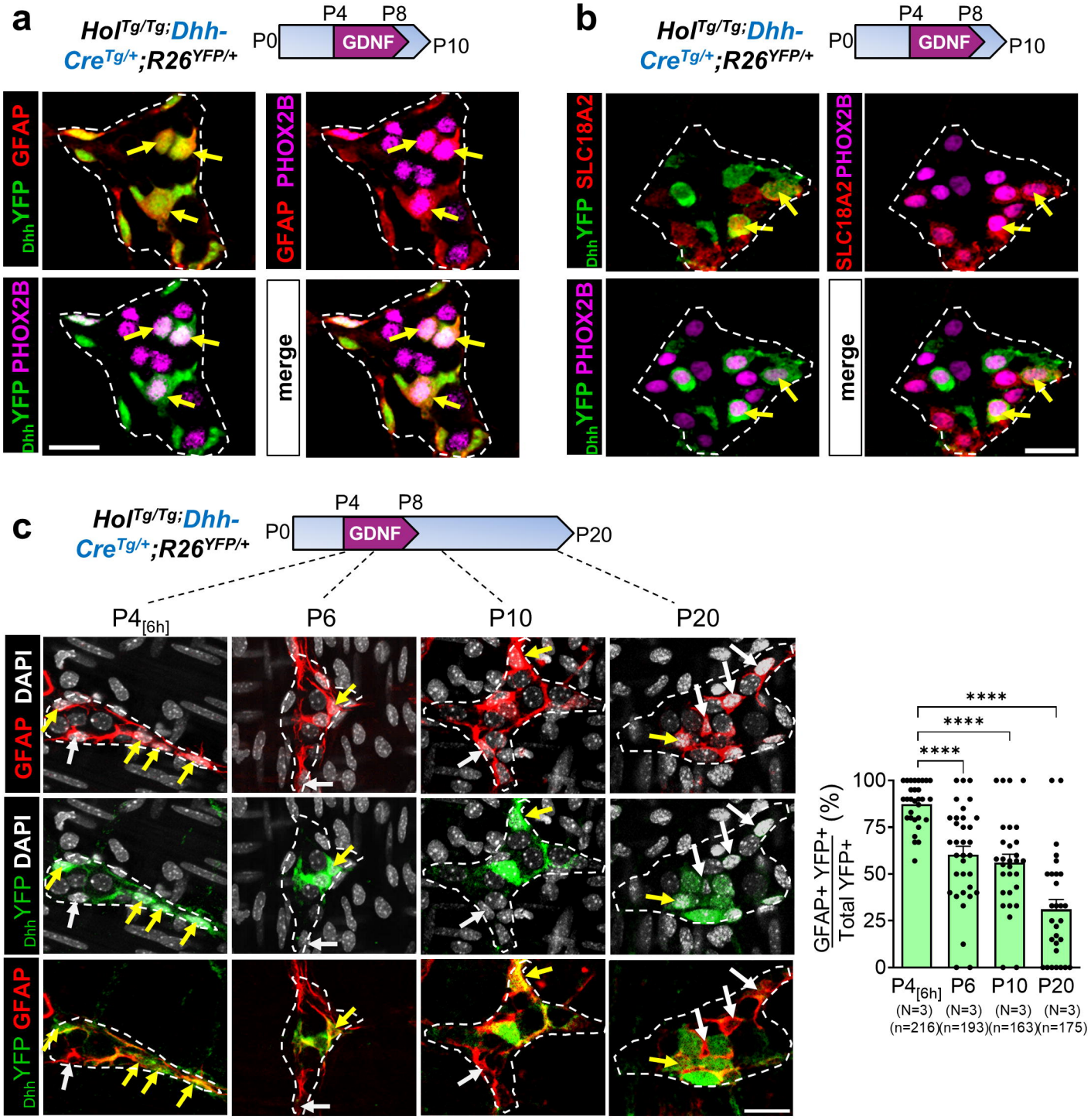
a
Hol Tg/Tg;Dhh-Cre Tg/+;R26 YFP/+
P0
P4
P8
GDNF
P10
Dhh YFP GFAP
GFAP PHOX2B
Dhh YFP PHOX2B
merge
b
Hol Tg/Tg;Dhh-Cre Tg/+;R26 YFP/+
P0
P4
P8
GDNF
P10
Dhh YFP SLC18A2
SLC18A2 PHOX2B
Dhh YFP PHOX2B
merge
c
Hol Tg/Tg;Dhh-Cre Tg/+;R26 YFP/+
P0
P4
P8
GDNF
P20
P4[6h]
P6
P10
P20
GFAP DAPI
Dhh YFP DAPI
Dhh YFP GFAP
****
****
****
GFAP+ YFP+ / Total YFP+ (%)
100
75
50
25
0
P4[6h]
P6
P10
P20
(N=3) (n=216)
(N=3) (n=193)
(N=3) (n=163)
(N=3) (n=175)

Fig. 5

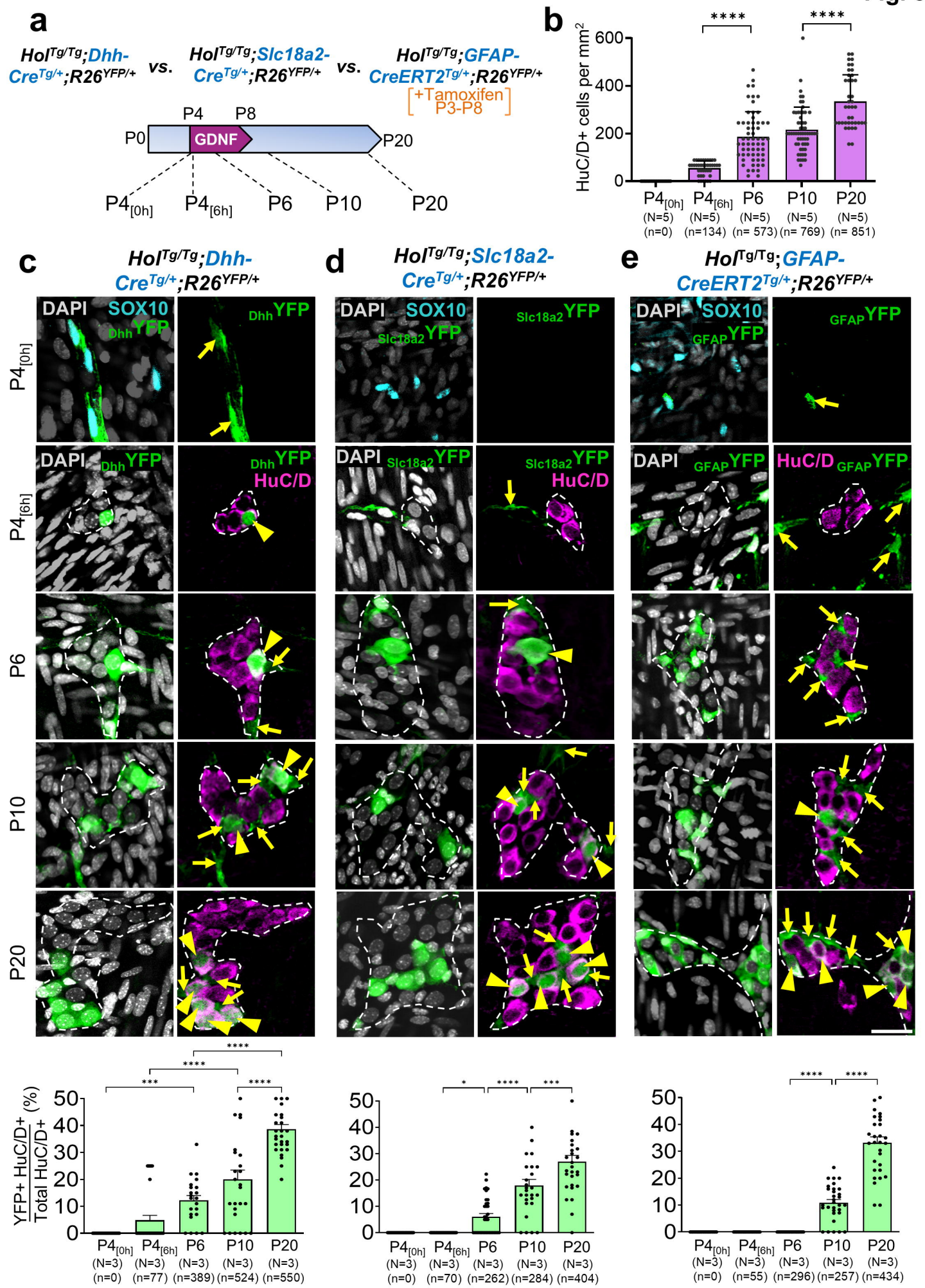
a
Hol Tg/Tg;Dhh-Cre Tg/+;R26 YFP/+ vs. Hol Tg/Tg;Slc18a2-Cre Tg/+;R26 YFP/+ vs. Hol Tg/Tg;GFAP-CreERT2 Tg/+;R26 YFP/+
[+Tamoxifen P3-P8]
P0
P4
P8
GDNF
P20
P4[0h]
P4[6h]
P6
P10
P20
b
HuC/D+ cells per mm2
600
400
200
0
****
****
P4[0h] (N=5) (n=0)
P4[6h] (N=5) (n=134)
P6 (N=5) (n= 573)
P10 (N=5) (n= 769)
P20 (N=5) (n= 851)
c
Hol Tg/Tg;Dhh-Cre Tg/+;R26 YFP/+
d
Hol Tg/Tg;Slc18a2-Cre Tg/+;R26 YFP/+
e
Hol Tg/Tg;GFAP-CreERT2 Tg/+;R26 YFP/+
P4[0h]
P4[6h]
P6
P10
P20
DAPI
SOX10
Dhh YFP
Slc18a2 YFP
GFAP YFP
HuC/D
YFP+ HuC/D+ / Total HuC/D+ (%)
50
40
30
20
10
0
***
****
****
*
****
***
****
****
P4[0h] (N=3) (n=0)
P4[6h] (N=3) (n=77)
P6 (N=3) (n=389)
P10 (N=3) (n=524)
P20 (N=3) (n=550)
P4[0h] (N=3) (n=0)
P4[6h] (N=3) (n=70)
P6 (N=3) (n=262)
P10 (N=3) (n=284)
P20 (N=3) (n=404)
P4[0h] (N=3) (n=0)
P4[6h] (N=3) (n=55)
P6 (N=3) (n=296)
P10 (N=3) (n=257)
P20 (N=3) (n=434)

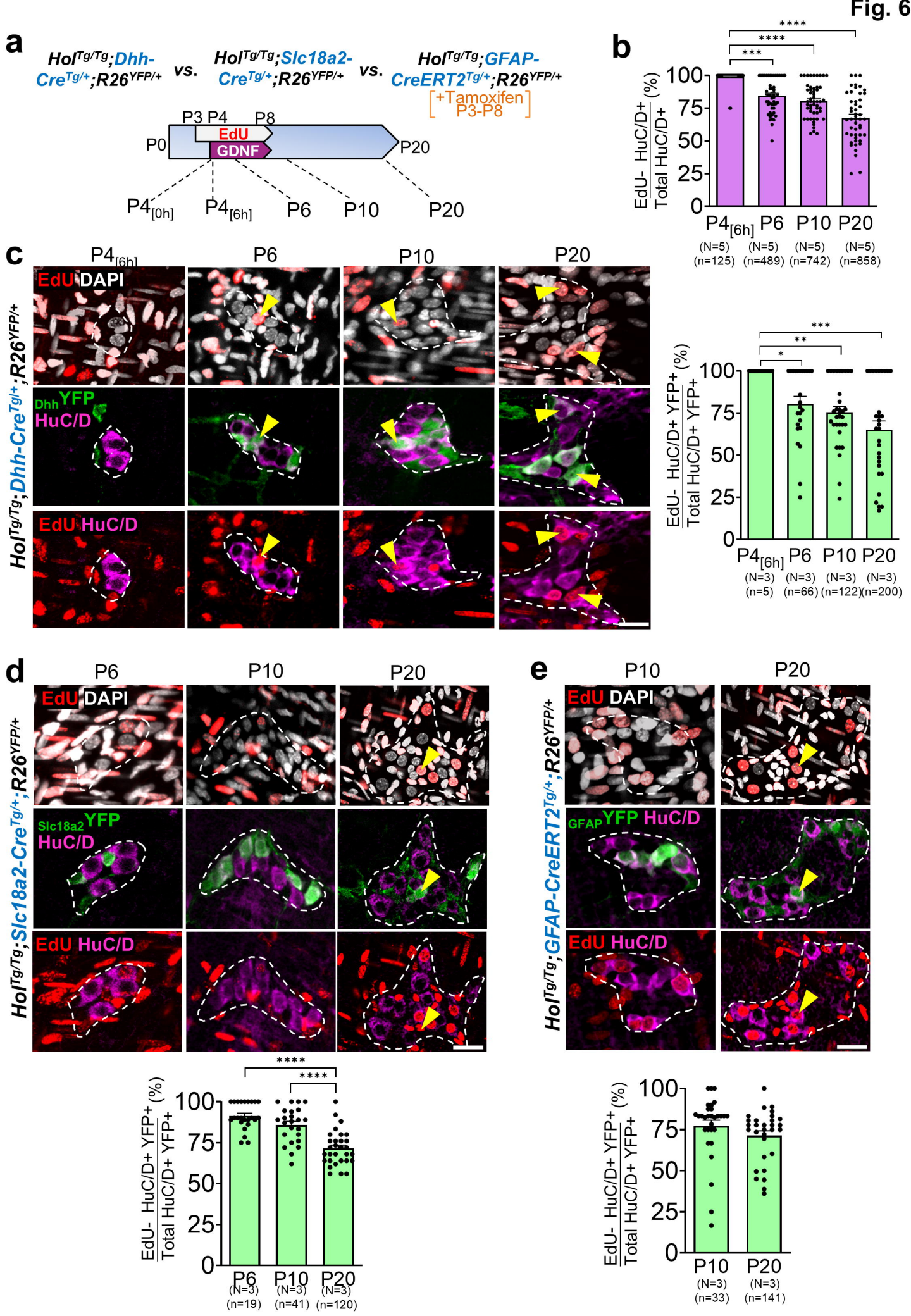
a
Hol Tg/Tg;Dhh-Cre Tg/+;R26 YFP/+
vs.
Hol Tg/Tg;Slc18a2-Cre Tg/+;R26 YFP/+
vs.
Hol Tg/Tg;GFAP-CreERT2 Tg/+;R26 YFP/+
[+Tamoxifen P3-P8]
P3 P4 P8
P0
EdU
GDNF
P20
P4[0h]
P4[6h]
P6
P10
P20
b
EdU- HuC/D+ / Total HuC/D+ (%)
P4[6h] P6 P10 P20
(N=5) (N=5) (N=5) (N=5)
(n=125) (n=489) (n=742) (n=858)
c
P4[6h]
P6
P10
P20
EdU DAPI
Dhh YFP
HuC/D
EdU HuC/D
Hol Tg/Tg;Dhh-Cre Tg/+;R26 YFP/+
EdU- HuC/D+ YFP+ / Total HuC/D+ YFP+ (%)
P4[6h] P6 P10 P20
(N=3) (N=3) (N=3) (N=3)
(n=5) (n=66) (n=122) (n=200)
d
P6
P10
P20
EdU DAPI
Slc18a2 YFP
HuC/D
EdU HuC/D
Hol Tg/Tg;Slc18a2-Cre Tg/+;R26 YFP/+
EdU- HuC/D+ YFP+ / Total HuC/D+ YFP+ (%)
P6 P10 P20
(N=3) (N=3) (N=3)
(n=19) (n=41) (n=120)
e
P10
P20
EdU DAPI
GFAP YFP HuC/D
EdU HuC/D
Hol Tg/Tg;GFAP-CreERT2 Tg/+;R26 YFP/+
EdU- HuC/D+ YFP+ / Total HuC/D+ YFP+ (%)
P10 P20
(N=3) (N=3)
(n=33) (n=141)

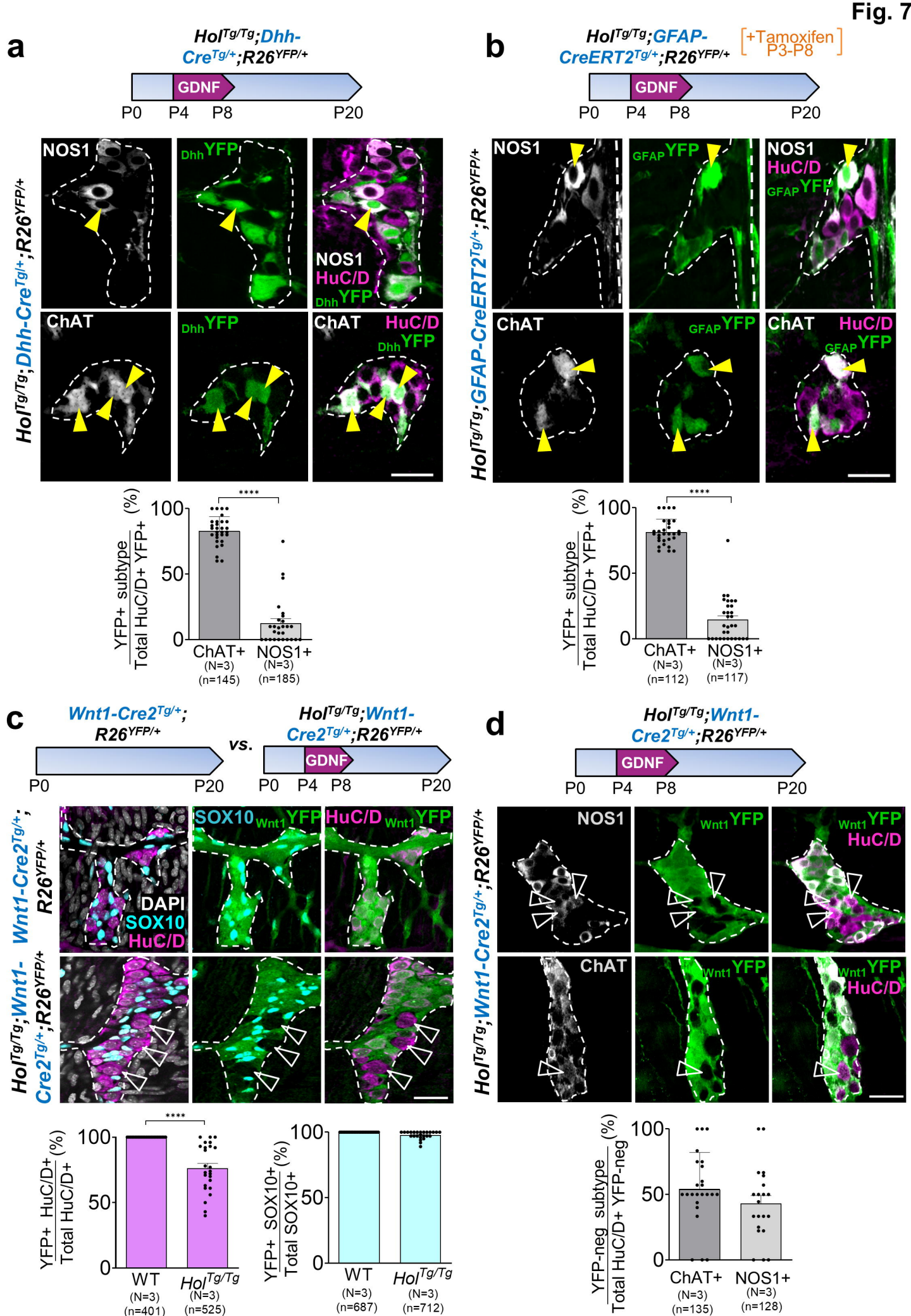
a
Hol Tg/Tg;Dhh-Cre Tg/+;R26 YFP/+
GDNF
P0 P4 P8 P20
NOS1
Dhh YFP
NOS1 HuC/D Dhh YFP
ChAT
Dhh YFP
ChAT HuC/D Dhh YFP
Hol Tg/Tg;Dhh-Cre Tg/+;R26 YFP/+
YFP+ subtype / Total HuC/D+ YFP+ (%)
100
50
0
****
ChAT+ (N=3) (n=145)
NOS1+ (N=3) (n=185)
b
Hol Tg/Tg;GFAP-CreERT2 Tg/+;R26 YFP/+
[+Tamoxifen P3-P8]
GDNF
P0 P4 P8 P20
NOS1
GFAP YFP
NOS1 HuC/D GFAP YFP
ChAT
GFAP YFP
ChAT HuC/D GFAP YFP
Hol Tg/Tg;GFAP-CreERT2 Tg/+;R26 YFP/+
YFP+ subtype / Total HuC/D+ YFP+ (%)
100
50
0
****
ChAT+ (N=3) (n=112)
NOS1+ (N=3) (n=117)
c
Wnt1-Cre2 Tg/+; R26 YFP/+
vs.
Hol Tg/Tg;Wnt1-Cre2 Tg/+;R26 YFP/+
GDNF
P0 P20
P0 P4 P8 P20
DAPI SOX10 HuC/D
SOX10 Wnt1 YFP
HuC/D Wnt1 YFP
Wnt1-Cre2 Tg/+; R26 YFP/+
Hol Tg/Tg;Wnt1-Cre2 Tg/+;R26 YFP/+
YFP+ HuC/D+ / Total HuC/D+ (%)
100
50
0
****
WT (N=3) (n=401)
Hol Tg/Tg (N=3) (n=525)
YFP+ SOX10+ / Total SOX10+ (%)
100
50
0
WT (N=3) (n=687)
Hol Tg/Tg (N=3) (n=712)
d
Hol Tg/Tg;Wnt1-Cre2 Tg/+;R26 YFP/+
GDNF
P0 P4 P8 P20
NOS1
Wnt1 YFP
Wnt1 YFP HuC/D
ChAT
Wnt1 YFP
Wnt1 YFP HuC/D
Hol Tg/Tg;Wnt1-Cre2 Tg/+;R26 YFP/+
YFP-neg subtype / Total HuC/D+ YFP-neg (%)
100
50
0
ChAT+ (N=3) (n=135)
NOS1+ (N=3) (n=128)

Fig. 8

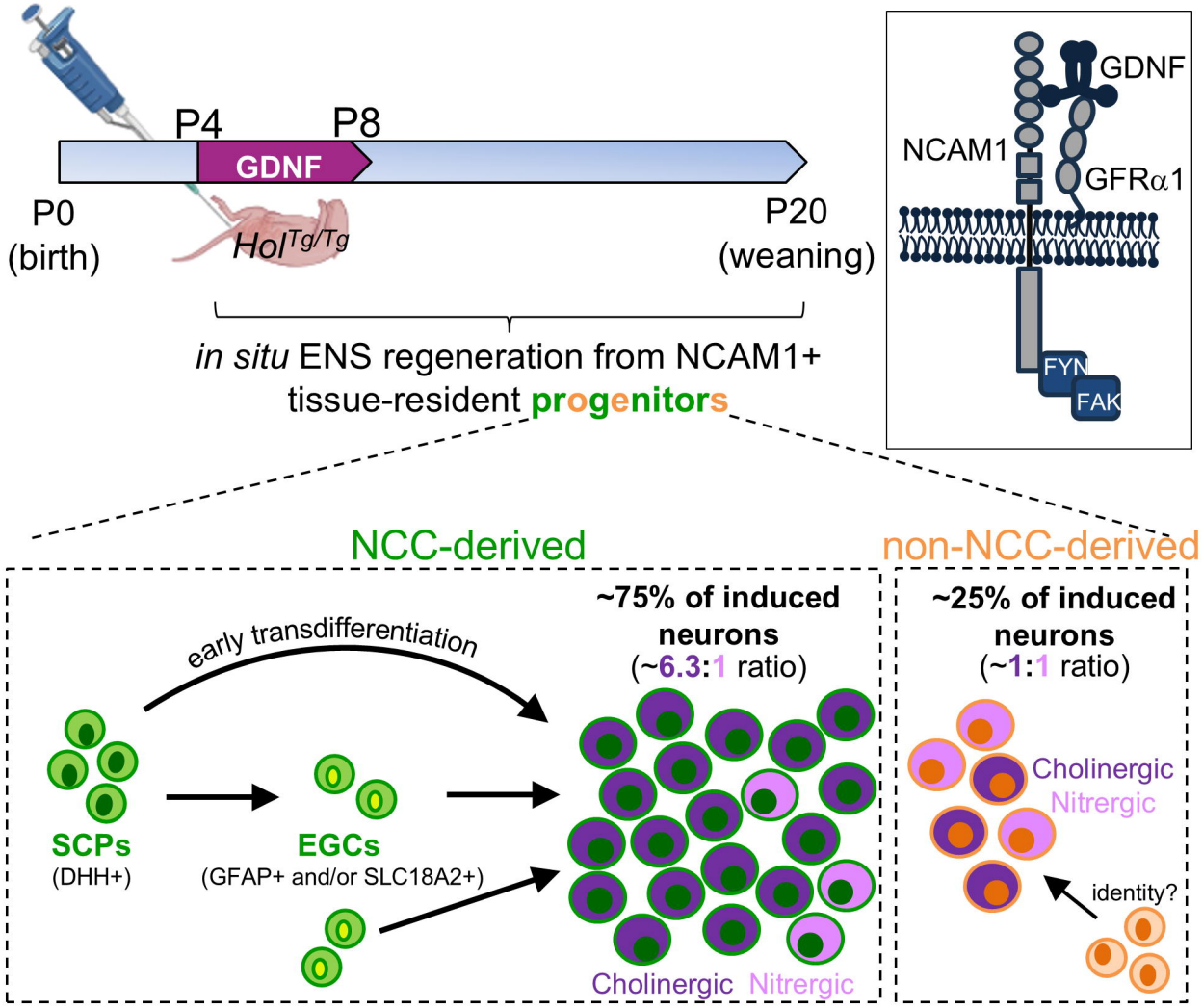
P4
P8
GDNF
P0
(birth)
Hol^Tg/Tg
P20
(weaning)
in situ ENS regeneration from NCAM1+
tissue-resident progenitors
GDNF
NCAM1
GFRα1
FYN
FAK
NCC-derived
non-NCC-derived
early transdifferentiation
~75% of induced
neurons
(~6.3:1 ratio)
~25% of induced
neurons
(~1:1 ratio)
SCPs
(DHH+)
EGCs
(GFAP+ and/or SLC18A2+)
Cholinergic
Nitrergic
Cholinergic
Nitrergic
identity?